JACS
JOURNAL OF THE AMERICAN CHEMICAL SOCIETY
pubs.acs.org/JACS
Article

Platinum(II) Di-ω-alkenyl Complexes as "Slow-Release" Precatalysts for Heat-Triggered Olefin Hydrosilylation

Sumeng Liu and Gregory S. Girolami*

Cite This: J. Am. Chem. Soc. 2021, 143, 17492−17509
Read Online
ACCESS | Metrics & More | Article Recommendations | Supporting Information

ABSTRACT: We describe the synthesis, characterization, and catalytic hydrosilylation activity of platinum(II) di-ω-alkenyl compounds of stoichiometry PtR_2, where R = CH_2SiMe_2(vinyl) (**1**) or CH_2SiMe_2(allyl) (**2**), and their adducts with 1,5-cyclooctadiene (COD), dibenzo[a,e]cyclooctatetraene (DBCOT), and norbornadiene (NBD), which can be considered as slow-release sources of the reactive compounds **1** and **2**. At loadings of 0.5 × 10^{-6}−5 × 10^{-6} mol %, **1-COD** is an active hydrosilylation catalyst that exhibits heat-triggered latency: no hydrosilylation activity occurs toward many olefin substrates even after several hours at 20 °C, but turnover numbers as high as 200000 are seen after 4 h at 50 °C, with excellent selectivity for formation of the anti-Markovnikov product. Activation of the Pt^{II} precatalyst occurs via three steps: slow dissociation of COD from **1-COD** to form **1**, rapid reaction of **1** with silane, and elimination of both ω-alkenyl ligands to form Pt^0 species. The latent catalytic behavior, the high turnover number, and the high anti-Markovnikov selectivity are a result of the slow release of **1** from **1-COD** at room temperature, so that the concentration of Pt^0 during the initial stages of the catalysis is negligible. As a result, formation of colloidal Pt, which is known to cause side reactions, is minimized, and the amounts of side products are very small and comparable to those seen for platinum(0) carbene catalysts. The latent reaction kinetics and high turnover numbers seen for **1-COD** after thermal triggering make this compound a potentially useful precatalyst for injection molding or solvent-free hydrosilylation applications.

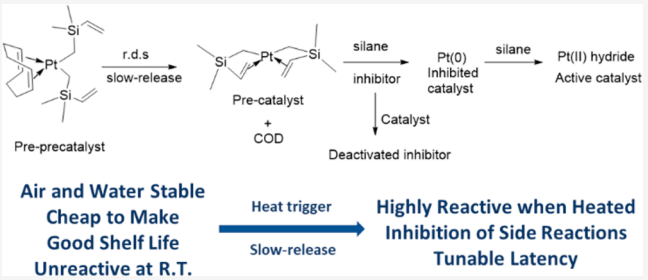

INTRODUCTION

Hydrosilylation reactions are widely employed in the production of functional polymers[1−6] and for applications such as automotive gaskets, paper release coatings, pressure sensitive adhesives, and injection molded parts.[7] The most widely used catalyst for these reactions is Karstedt's catalyst, a molecular Pt^0 tris(olefin) complex.[4,6,8] This catalyst is highly reactive: turnover rates of millions/hour are often seen.[9] Related compounds known as Markó's catalysts, in which one of the three olefin ligands is replaced with an *N*-heterocyclic carbene, offer enhanced selectivity for the desired anti-Markovnikov addition product with some loss of activity.[10,11]

Although complexes of other metals are known to be active for the hydrosilylation of olefins,[1,6] platinum is the current choice for industrial hydrosilylation catalysis because of its high reactivity and tolerance to a variety of process conditions.

One major challenge in making cross-linked silicones by hydrosilylation is to design catalytic systems that exhibit near-zero rates under ambient conditions, but very fast rates during the curing step, with low catalyst loadings.[1,2] Such an advance would simplify the manufacturing process because the end user would not need to add the catalyst to the formulation. The low catalyst loadings are required so as to reduce catalyst costs and—because the catalysts generally cannot be removed after curing—to minimize color in the product.

Several strategies have been adopted to achieve these goals, including the use of catalyst inhibitors, catalyst encapsulants, photogenerated catalysts, and dormant precatalysts; such systems are inactive until triggered by heat or light.[1,2] All these approaches have their limitations, and the problem becomes especially challenging when the required curing temperature is low (<100 °C).

We describe here our efforts to carry out hydrosilylation catalysis at low temperatures (≤100 °C) and low precatalyst loadings, with the goal of developing a system that shows latency: the catalytic activity is near-zero at room temperature but very high when thermally triggered. Our approach is to employ a Pt^{II} compound that does not convert into an active catalyst[9] at room temperature (or does so very slowly) but when heated converts quickly and efficiently to a Karstedt-like molecular Pt^0 species by a "slow-release"[12] process.

Received: July 4, 2021
Published: October 13, 2021

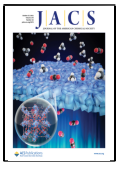

https://doi.org/10.1021/jacs.1c06846
J. Am. Chem. Soc. 2021, 143, 17492−17509

In our implementation of this concept, we designed compounds of stoichiometry $PtR_2(COD)$, which is a precatalyst (PtR_2) that is bound to a strongly coordinating inhibitor, in this case 1,5-cyclooctadiene (COD). We chose the R groups to be vinyl- and allyl-substituted neosilyl groups, $CH_2SiMe_2CH{=}CH_2$ and $CH_2SiMe_2CH_2CH{=}CH_2$. The steric hindrance of these ω-alkenyl groups disfavors the reaction of $PtR_2(COD)$ with silane,[13] but the presence of the terminal vinyl or allyl groups promotes the conversion of the $PtR_2(COD)$ compounds (in which the ligands are unidentate) into PtR_2 compounds (in which they are bidentate); the latter are highly reactive and efficiently convert into the actual catalyst (Scheme 1).

Scheme 1. Generation of the Pt^{II} Hydride Catalyst from $PtR_2(COD)$[a]

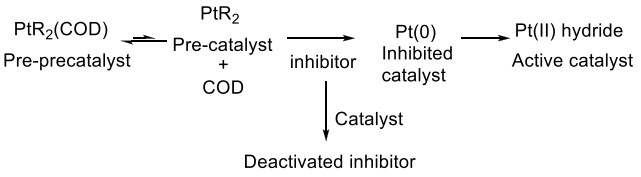

[a]The inhibitor either inhibits the formation of Pt^0 species or inhibits the Pt^0 species after they are formed.

Such an activation mechanism has several advantages: First, the relatively "slow-release"[12] nature of catalyst generation reduces the concentration of active catalyst in solution and, thus, disfavors association of the monomeric catalytic centers into colloidal Pt particles; the latter are known to catalyze undesirable side reactions such as olefin isomerization and hydrogenation.[14] Second, the multiple-step activation process allows fine-tuning of the activation kinetics, for example, by addition of consumable inhibitors that increase the latency. Whereas inhibitors are widely used in industrial hydrosilylation catalysis,[1] the effect of inhibition is more effective in the present design because the target of the inhibitor is only a small fraction of the metal centers (those that have been "released"). Finally, in this catalytic system, the overall reaction kinetics can be made autoinductive (in an autoinductive reaction, the reaction products increase the reactivity of the catalyst, rather than directly converting reactants to products)[15] through the use of consumable inhibitors, so that the catalytic rate accelerates quickly at the end of the latency period.

We will show that this strategy results in catalysts that are inactive for hydrosilylation over several hours at ~20 °C, whereas catalytic turnovers as high as 200000 are seen over 30 min at 50 °C. We show that our compounds, much like Markó's catalyst,[10,11] achieve excellent product regioselectivities and generate minimal amounts of undesired side-products.

RESULTS AND DISCUSSION

Synthesis of the Platinum Precatalysts. Treatment of $PtCl_2(SMe_2)_2$ with 2 equiv of a dimethyl(vinyl)silylmethyl or dimethyl(allyl)silylmethyl Grignard reagent generates the new homoleptic platinum(II) compounds PtR_2, where R is $-CH_2SiMe_2CH{=}CH_2$ (**1**) or $-CH_2SiMe_2CH_2CH{=}CH_2$ (**2**). Compound **1** is a low-melting, thermally sensitive liquid that darkens within a few hours at room temperature under argon; compound **2** is a low-melting, thermally sensitive solid that decomposes within a week at room temperature under argon.

Similar treatment of the 1,5-cyclooctadiene starting material $PtCl_2(COD)$ gives related platinum(II) ω-alkenyl complexes of stoichiometry $PtR_2(COD)$ where R is $-CH_2SiMe_2CH{=}CH_2$ (**1-COD**) or $-CH_2SiMe_2CH_2CH{=}CH_2$ (**2-COD**). Both compounds are colorless liquids, stable toward air and water, and can be stored indefinitely at −20 °C in air. Both compounds are highly soluble in organic solvents and silicone oligomers. A TGA experiment shows that **1-COD** decomposes thermally at ~100 °C. As expected, the vinyl and allyl groups on silicon are coordinated to Pt in the PtR_2 compounds **1** and **2** but are not coordinated to Pt in the adducts **1-COD** and **2-COD** (see below).

An alternative way to synthesize **1-COD** is by treatment of the PtR_2 complex **1** with COD; **1** reacts similarly with dibenzo[*a*,*e*]cyclooctatetraene (DBCOT) to form **1-DBCOT** and with norbornadiene to generate the adduct **1-NBD** (Scheme 2).

Scheme 2. Synthesis of Platinum(II) ω-Alkenyl Complexes

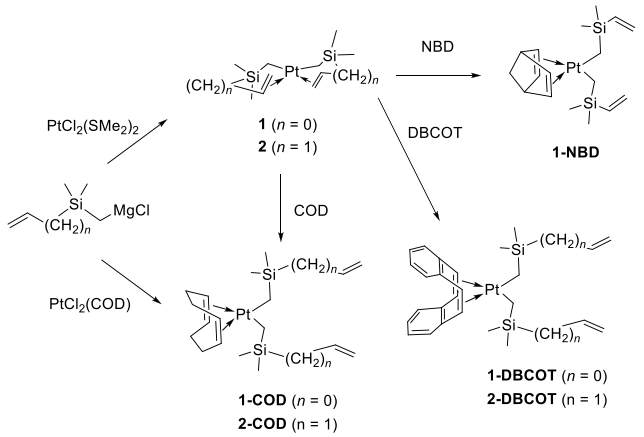

Unlike **1-COD** or **1-DBCOT**, however, **1-NBD** is heat- and air-sensitive: it darkens in air within several minutes at room temperature. Similarly, treatment of the allylic PtR_2 compound **2** with DBCOT generates **2-DBCOT**. Unidentate olefins (such as cyclooctene), acyclic dienes (such as 1,3-divinyltetramethyldisiloxane), and alkynes (such as diphenylacetylene) do not form isolable adducts with **1**. Compounds **1-COD**[16] and **1-NBD**[17] have been described previously; the other compounds described here are new.

Crystal Structure of the PtR_2 Complex 2. Single crystals of the PtR_2 compound **2** (whose Si atoms bear allyl groups) suitable for an X-ray diffraction study were grown by concentrating a pentane solution of **2** at −78 °C. Crystal data are given in Table S10.1, and bond distances and angles are summarized in Table 1. Like its carbon analogue $Pt(CH_2CMe_2CH_2CH{=}CH_2)_2$, $\mathbf{2}^{C}$,[18] compound **2** is monomeric in the solid state (Figure 1). The Pt center is attached to two ω-alkenyl ligands in which the α-carbon atom is σ-bound to platinum (η^1) and the C=C bond at the other end of the chain is π-bound (η^2). The C=C bond distance of 1.360(6) Å is similar to the 1.366(3) Å distance seen for $\mathbf{2}^{C}$; the distance is relatively short for a coordinated olefin (Table 1) and suggests that the C=C bond is weakly coordinated to Pt. The Pt−olefin bonding is slightly unsymmetric: the $Pt{-}C_{olefin}$ distances to the methine and methylene carbon atoms in **2** differ by 0.11 Å and are longer by 0.07 and 0.04 Å, respectively, than the $Pt{-}C_{olefin}$ distances in the carbon analogue $\mathbf{2}^{C}$.

https://doi.org/10.1021/jacs.1c06846
J. Am. Chem. Soc. 2021, 143, 17492−17509

Table 1. Selected Bond Distances for Some PtR_2 and $PtR_2(COD)$ Complexes[a]

	2	2[C][18]	3-COD[19]	1-DBCOT	2-DBCOT	4
alkenyl C=C (Å)	1.360(6)	1.366(3)	N/A	1.328(5)	1.315(6)	1.374(5)
Pt−C_α (Å)	2.065(4)	2.058(2)	2.070(8)	2.068(3)	2.056(3)	2.077(3)
Pt−C_{olefin}[b] (Å)	2.370(4)	2.301(2)	N/A	N/A	N/A	2.267(3)
Pt−C_{olefin}[c] (Å)	2.266(4)	2.250(2)	N/A	N/A	N/A	2.258(3)
C_α−Si_β (Å)	1.842(4)	1.544(7)	1.870 (10)	1.873(3)	1.864(4)	1.870(3)
Si_β−C_γ (Å)	1.888(5)	1.534(8)	1.870 (10)	1.876(4)[e]	1.893(5)	1.878(3)
C_γ−Si_δ (Å)	N/A	N/A	N/A	N/A	N/A	1.856(3)
Pt−C_α−Si_β (deg)	104.1(4)	110.7(5)	115.1(4)	113(1)	117 (1)	112.0(8)
C_α−Si_β−C_γ[d] (deg)	100.7(2)	106.6(2)	N/A	112(2)	109(1)	108.3(6)

[a]Some of the numbers given are averages over chemically equivalent bonds. [b]Methine carbon. [c]Methylene carbon. [d]C_α−C_β or C_β−C_γ bond. [e]Me−Si bond.

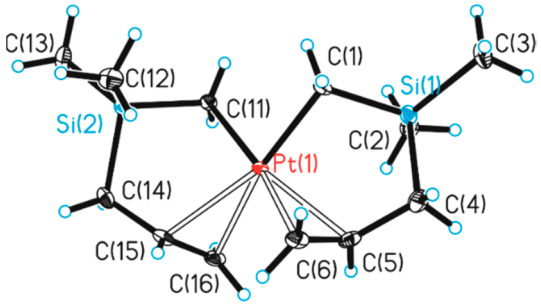

Figure 1. Crystal structure of $Pt(CH_2SiMe_2CH_2CH{=}CH_2)_2$ (**2**). Ellipsoids are drawn at the 35% probability level.

Some of the differences between the structure of **2** and that of the carbon analogue $\mathbf{2}^C$ arise from the presence of the larger silicon atom. Owing to the larger bite size of the chelating ring, the C=C bonds are tilted by only 15° from being perpendicular to the Pt square plane (vs 30° in $\mathbf{2}^C$). The C_α−Si−C_γ bond angle of 100.7(2)° in **2** is significantly smaller than the C_α−C_β−C_γ bond angle of 106.6(2)° in $\mathbf{2}^C$; the closing of this angle shows that the silicon atom accommodates more of the ring strain caused by the chelation of the ω-alkenyl ligand. For similar reasons, the Pt−C_α−Si bond angle of 104.1(4)° in **2** is smaller than the Pt−C_α−C_β bond angle of 110.7(5)° in $\mathbf{2}^C$.

Interestingly, the Si−C bond distances in **2** are not all the same: the Si−C_α distance of 1.842(4) Å is very slightly shorter than the Si−Me bond distances of 1.872(5) Å. This small variation in the Si−C_α distances may indicate the presence of a hyperconjugation effect: the small Pt−C_α−Si bond angle of 104° means that the Pt−C_α and C_α−Si bonds are nearly perpendicular to one another. As a result, the Pt−C_α σ and σ* orbitals can mix with other Si−C bonding or antibonding orbitals of π-symmetry with respect to the C_α−Si bond axis through an α-silicon effect,[20−23] so that the Si−C_α bond acquires partial double bond character. This effect can be represented as follows, in which the hyperconjugated resonance form corresponds to a platinum(II) allyl/silene structure:

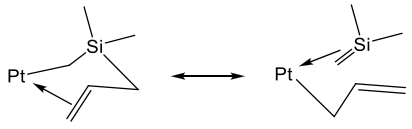

Although the structural consequences of this α-silicon effect are small (i.e., the hyperconjugated resonance form is at best a very minor contributor to the electronic structure), these changes in the Si−C bond lengths may be relevant to the mechanism by which **1**, **2**, and some related compounds[24] decompose when heated, as we will discuss below.

Crystal Structures of the Adducts 1-DBCOT and 2-DBCOT. Single crystals of the dibenzo[*a*,*e*]cyclooctatetraene adducts **1-DBCOT** and **2-DBCOT** were grown from pentane at −20 °C and from its melt at 4 °C, respectively (see the Supporting Information). Crystal data are given in the Supporting Information, and selected bond distances and angles are summarized in Table 1. In these two compounds, the ω-alkenyl groups are unidentate as expected (Figure 2). In the vinyl compound **1-DBCOT**, the Si−Me and Si−CH_2 bond distances are all normal (1.870(10) Å), as seen in the closely related compound $Pt(CH_2SiMe_3)_2(COD)$,[19] which we will refer to as **3-COD**. The Pt−C_α−Si bond angle of 117(1)° in **2-DBCOT** is

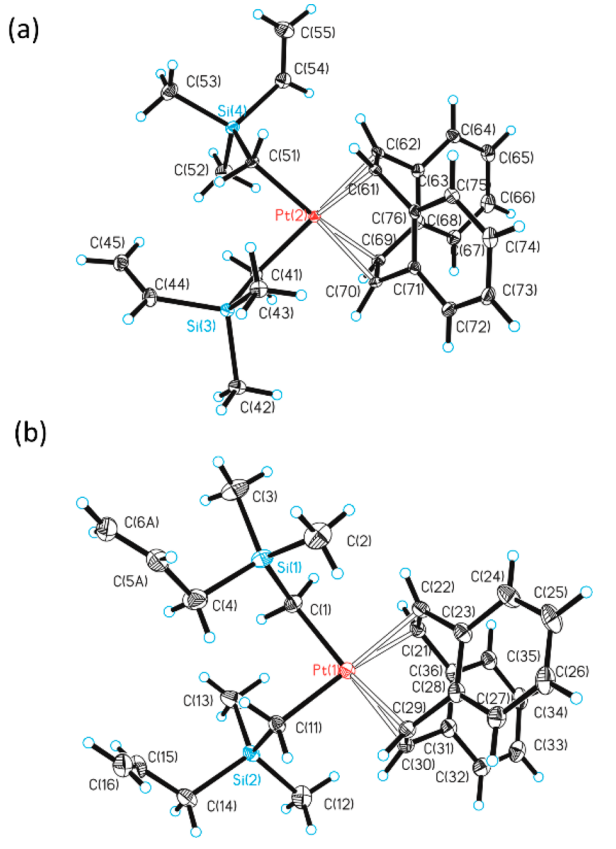

Figure 2. Crystal structures of (a) (DBCOT)$Pt(CH_2SiMe_2CH{=}CH_2)_2$ (**1-DBCOT**) and (b) (DBCOT)$Pt(CH_2SiMe_2CH_2CH{=}CH_2)_2$ (**2-DBCOT**). Ellipsoids are drawn at the 35% probability level.

https://doi.org/10.1021/jacs.1c06846
J. Am. Chem. Soc. 2021, 143, 17492−17509

similar to those of 112(2)° in **1-DBCOT** and 115.1(4)° in the CH_2SiMe_3 compound **3-COD**. These large angles, and the absence of the shortening of the Si−C_α bond, are consistent with the conclusion that an α-silicon effect contributes to the thermal instability of **1**, **2**, and some related compounds (see below).[24]

Solution Properties of the PtR_2 Compounds 1 and 2. In solution, the PtR_2 compounds **1** and **2** both exhibit two resonances in the ^{195}Pt NMR spectra, which are present in a ~7:1 ratio for the Si−vinyl complex **1** and a ~2:1 ratio for the Si−allyl complex **2** (Figure 3). The carbon analogues also exist

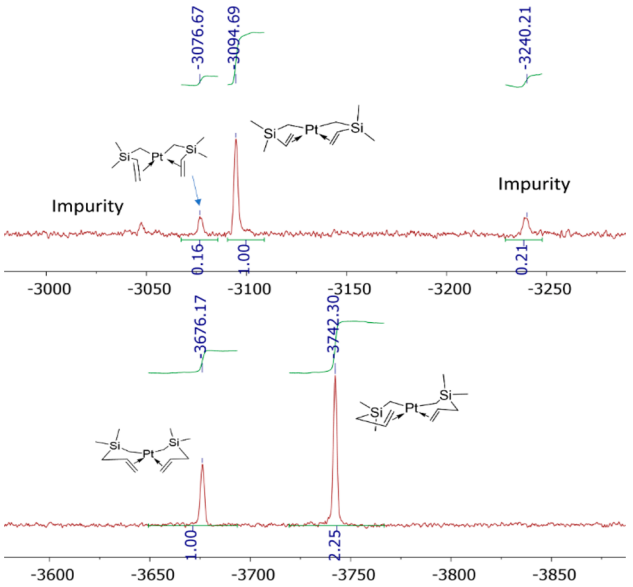

Figure 3. (Top) ^{195}Pt{^{1}H} NMR spectrum of $Pt(CH_2SiMe_2CH{=}CH_2)_2$ (**1**) at 0 °C in toluene-d_8. (Bottom) ^{195}Pt NMR spectrum of $Pt(CH_2SiMe_2CH_2CH{=}CH_2)_2$ (**2**) at 20 °C in toluene-d_8. For both compounds, two isomers (C_2 and C_s) exist in solution.

in solution as a mixture two isomers in solution, one of C_2 symmetry and one of C_s symmetry.[18] In the carbon analogues, the minor C_s isomer is more stable if the chain is short (four atoms, so that the two olefin groups are far apart) or long (six atoms, so that the two olefinic groups can orient perpendicular to the Pt square plane). For five-atom chain lengths, the C_s isomer is disfavored because the chains are long enough for the two olefin groups to clash sterically but not long enough for them to twist into a conformation perpendicular to the square-planar coordination environment of the metal center.

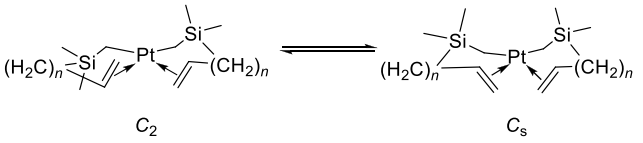

Relative to the carbon analogue **2**^{C}, the larger bite angle for the ligands in **2** enables the olefin C═C vector to orient more nearly perpendicular to the Pt square plane. This difference reduces the steric clashing between the olefinic groups in **2**, which makes the energies of the C_2 and C_s isomers more similar: the C_2:C_s ratio is 2:1 for **2** vs >100:1 for **2**^{C}. In contrast, the larger bite angle for the ligands in **1** vs **1**^{C} brings the two olefinic groups closer to one another so that they interact more strongly and make the energies of the C_2 and C_s isomers more different: the C_2:C_s ratio is 7:1 for **1** vs 2:1 for **1**^{C}.

The presence of two isomers for both **1** and **2** is also evident in their low-temperature ^{1}H and ^{13}C{^{1}H} NMR spectra, which contain two sets of well-resolved sharp peaks in the same ratios as seen in the ^{195}Pt NMR spectra (Table 2). The shielded chemical shifts for the olefinic ^{1}H and ^{13}C NMR resonances, the nonzero ^{195}Pt couplings to these olefinic resonances, the diminished ^{1}H−^{1}H couplings between the olefinic protons relative to free olefins, and the diastereotopic nature of the $SiMe_2$ groups clearly show that the terminal C═C bonds in both isomers of **1** and **2** are coordinated to Pt.

Variable-temperature ^{1}H NMR studies show that there is a very small temperature dependence of the equilibrium constant $K_{eq} = [C_s]/[C_2]$, in which concentration of the minor (C_s) isomer of both **1** and **2** increases with temperature. Fitting the data for the Si-vinyl compound **1** to the van't Hoff equation gives $\Delta H = 0.5 \pm 1.7$ kcal mol^{-1}, $\Delta S = -1 \pm 7$ cal mol^{-1}·K^{-1} (Figure 4). The Si-allyl compound **2** shows almost identical behavior: $\Delta H = 0 \pm 0.5$ kcal mol^{-1}, $\Delta S = -1 \pm 2$ cal mol^{-1}·K^{-1} (Figure 5).

As discussed for carbon analogues,[18] the C_2 and C_s isomers of **1** and **2** interconvert in solution by means of an "alkene flipping" process[25] in which the olefin decomplexes from the Pt center and recoordinates through the other face of the olefin.[26,27] For **1**, the rate of the olefin face exchange process was measured by spin saturation transfer. A fit of six rates between −23 and +2 °C to the Eyring equation gives activation parameters of $\Delta H^{\ddagger} = 17 \pm 2$ kcal mol^{-1} and $\Delta S^{\ddagger} = 10 \pm 9$ cal mol^{-1}·K^{-1} for olefin decomplexation of the C_2 isomer (Figure 4). The enthalpy of

Table 2. Selected ^{1}H and ^{13}C NMR Data for the Alkenyl Ligands in 1, 2, 1-COD, 1-NBD, and 2-COD

	1[a]	**2**[b]	**1-COD**[c]	**1-NBD**[c]	**1-DBCOT**[c]	**2-COD**[c]	**2-DBCOT**[c]
^{1}H δ (α-CH_2)	1.30, 0.18	1.44, 0.68	1.18	1.31	1.36	1.08	1.29
^{1}H $^2J_{PtH}$ (α-CH_2) (Hz)	71, 90	37, 102	92.9	102.2	93.0	93.4	93.6
^{1}H δ (−CH═)	4.23	4.74	6.52	6.52	6.49	6.07	6.04
^{1}H δ (═CH_2)	4.27, 3.58	3.31[d], 3.51	6.00, 5.84	6.02, 5.85	5.95, 5.79	5.03	5.00
^{1}H $^3J_{HH}$ (olefinic) (Hz)	18.0, 11.2	16[d], 8.6	20.2, 14.5	20.2, 14.5	20.3, 14.5	multiplet	multiplet
^{13}C δ (α-CH_2)	−0.79	15.68	11.75	14.89	20.25	11.52	19.83
^{13}C $^1J_{PtC}$ (α-CH_2) (Hz)	557	726	704.9	748.8	694.9	706.5	694.0
^{13}C δ (−CH═)	90.44	114.05	144.60	144.64	143.87	136.97	136.66
^{13}C δ (═CH_2)	93.10	83.05	128.94	129.22	129.58	112.29	112.61
^{13}C $^1J_{PtC}$ (−CH═) (Hz)	~8	15	27.0[e]	29.6[e]	24[e]	0	0
^{13}C $^1J_{PtC}$ (═CH_2) (Hz)	46	49	0	0	0	0	0

[a]For the major (C_2) isomer in toluene-d_8 at −50 °C. [b]For the major (C_2) isomer in toluene-d_8 at −30 °C. [c]In benzene-d_6 at room temperature. [d]Overlaps with a resonance from the minor isomer. [e]This is a three-bond coupling ($^3J_{PtC}$).

https://doi.org/10.1021/jacs.1c06846
J. Am. Chem. Soc. 2021, 143, 17492−17509

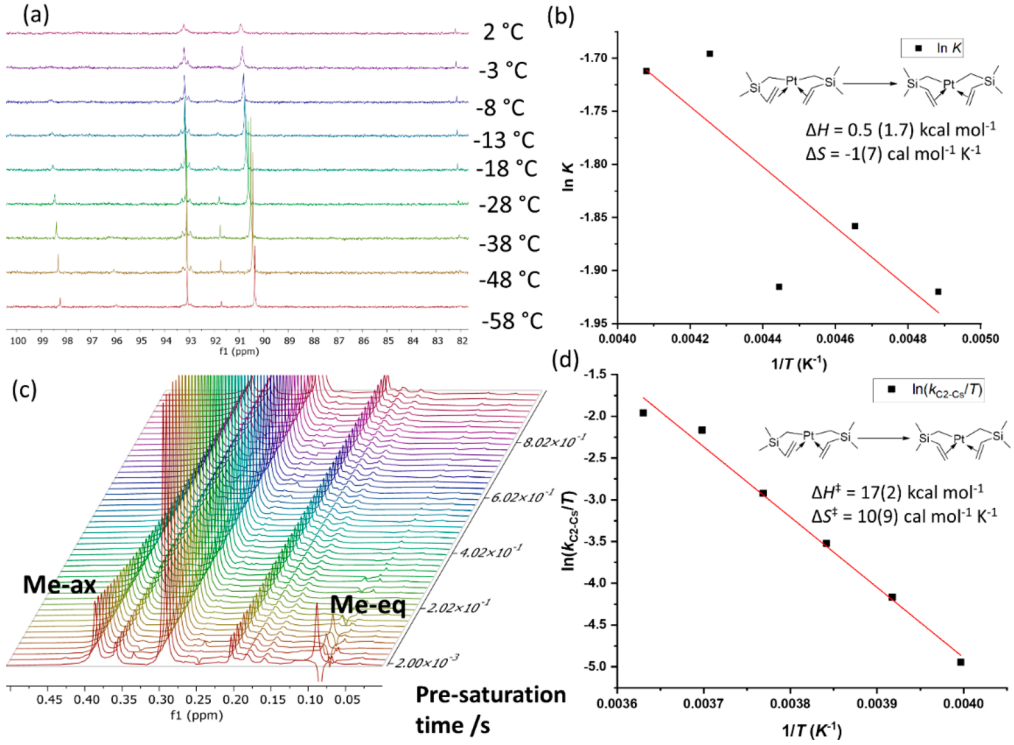

Figure 4. (a) Variable-temperature $^{13}C\{^1H\}$ NMR spectra of the olefinic carbons of *cis*-$Pt(CH_2SiMe_2CH{=}CH_2)_2$ (**1**) in toluene-d_8. (b) van 't Hoff plot for isomerization of **1** in toluene-d_8. Owing to peak overlap in the ^1H NMR spectra, the equilibrium constants are measured from $^{13}C\{^1H\}$ NMR spectra at low temperatures (−28 to −68 °C). The lower signal-to-noise ratio of the peak integrals is the cause of the scatter in the points. (c) Spin saturation transfer results at −18 °C showing decay of the axial methyl resonance of the C_2 isomer of **1** as a function of the presaturation time for irradiation of the equatorial methyl resonance. (d) Eyring plot of the rate of the conversion of the C_2 isomer to C_s isomer of **1** in toluene-d_8.

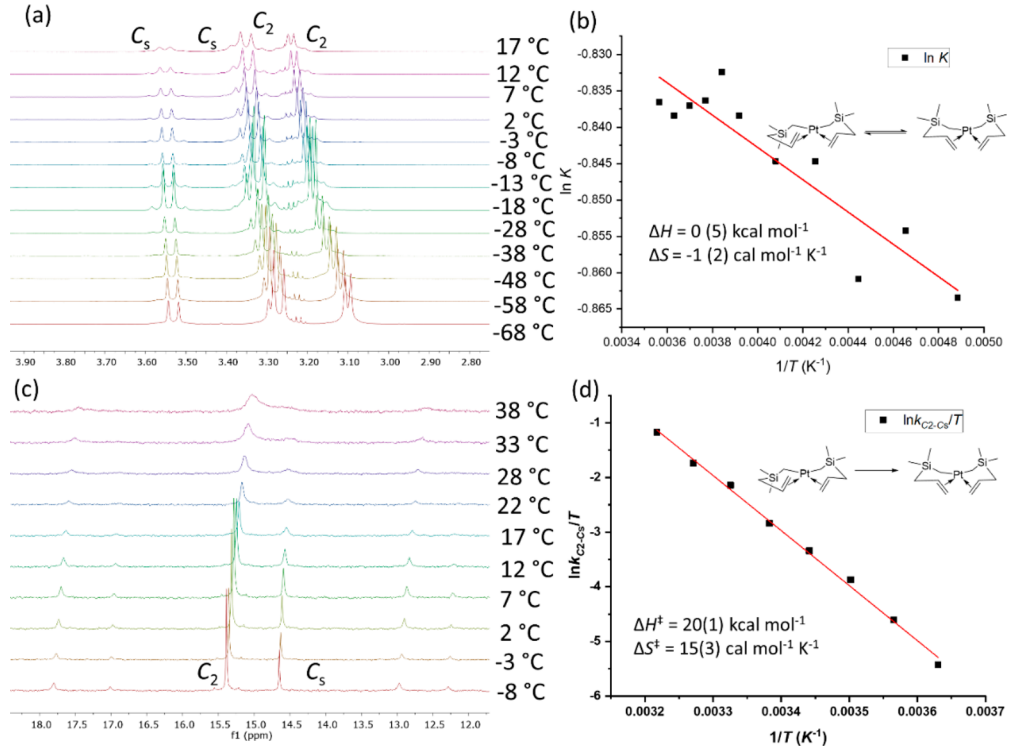

Figure 5. (a) Variable-temperature ^1H NMR spectra of the olefinic protons of $Pt(CH_2SiMe_2CH_2CH{=}CH_2)_2$ (**2**) in toluene-d_8. (b) van 't Hoff plot for the equilibrium between the C_2 and C_s isomers of **2**. (c) VT-$^{13}C\{^1H\}$ NMR spectra of α-CH_2 carbons of **2** in toluene-d_8. (d) Eyring plot of the rate of the conversion of the C_2 isomer to C_s isomer of **2** in toluene-d_8.

https://doi.org/10.1021/jacs.1c06846
J. Am. Chem. Soc. 2021, 143, 17492−17509

Table 3. Hydrosilylation of Allyl Glycidyl Ether (AGE) with $Pt(CH_2SiMe_2CH{=}CH_2)_2(COD)$ (1-COD), $Pt(CH_2SiMe_2CH_2CH{=}CH_2)_2(COD)$ (2-COD), and $Pt(CH_2SiMe_3)_2(COD)$ (3-COD) as the Precatalyst

entry	catalyst	silane	mol olefin/mol silane	cat. loading (10^{-6} mol %)	temp (°C)	conv of silane
1	**1-COD**	$HSiEt_3$	2	50	17	NR after 1 h
2	**2-COD**	$HSiEt_3$	2	50	17	NR after 1 h
3	**3-COD**	$HSiEt_3$	2	50	17	NR after 1 h
4	**1-COD**	$HSiEt_3$	2	50	60	82% after 1 h, 99% after 2 h
5	**2-COD**	$HSiEt_3$	2	50	60	64% after 1 h, 99% after 2 h
6	**3-COD**	$HSiEt_3$	2	50	60	12% after 2 h
7	**1-COD**	MD′M	2	50	17	<5% after 24 h
8	**1-COD**	MD′M	1	50	17	NR after 30 min, 4% after 4 h, 100% after 24 h
9	**2-COD**	MD′M	2	50	17	NR after 30 min, 5% after 4 h, 48% after 24 h
10	**1-COD**	MD′M	2	5	50	73% after 30 min, 100% after 4 h
11	**2-COD**	MD′M	2	5	50	~NR after 30 min, 10% after 4 h, 13% after 24 h
12	**2-COD**	MD′M	2	50	50	71% after 30 min, 100% after 4 h

activation is somewhat larger than the ~14 kcal mol^{-1} for the carbon analogue $Pt(CH_2CMe_2CH{=}CH_2)_2$, **1**$^{\mathbf{C}}$, whereas the entropy of activation is similar to the small and positive value of $\Delta S^{\ddagger} = 4 \pm 2$ cal $mol^{-1}{\cdot}K^{-1}$ for **1**$^{\mathbf{C}}$.[18]

The rate of the olefin face exchange process for **2** was determined by fitting the line shapes of selected $^{13}C\{^1H\}$ NMR resonances (see the Supporting Information). Fitting of the olefin face exchange rate at eight different temperatures between 2 and 38 °C to the Eyring equation gives $\Delta H^{\ddagger} = 20 \pm 1$ kcal mol^{-1} and $\Delta S^{\ddagger} = 15 \pm 3$ cal $mol^{-1}{\cdot}K^{-1}$ for the C_2 isomer (Figure 5). The activation parameters are similar to the $\Delta H^{\ddagger} = 19 \pm 1$ kcal mol^{-1} and $\Delta S^{\ddagger} = 10 \pm 3$ cal $mol^{-1}{\cdot}K^{-1}$ values seen for carbon analogue **2**$^{\mathbf{C}}$.[18] Similarly small but positive activation entropies of 12−14 cal $mol^{-1}{\cdot}K^{-1}$ seen for olefin face exchange processes in some 4-pentenyl zirconocene compounds were proposed to indicate a mechanism in which the metal-olefin bond is broken without concomitant association of solvent molecules.[28,29]

The rate of olefin decomplexation from the C_2 isomer at 0 °C is about 30 s^{-1} for **1** and about 3 s^{-1} for **2**, vs about 500 s^{-1} for **1**$^{\mathbf{C}}$ and 1 s^{-1} for **2**$^{\mathbf{C}}$. For the carbon analogues, the thermal stability is closely correlated with the relative rate of olefin decomplexation (faster decomplexation rates mean lower thermal stability). When gauged by this correlation, **1** and **2** are much more thermally sensitive than expected from their relatively low rates of olefin decomplexation. This difference is relevant to one possible mechanism for catalyst activation: the conversion of **1** and **2** to Pt^0 species.

Solution Properties of the PtR_2(COD), PtR_2(NBD), and PtR_2(DBCOT) Compounds. For the PtR_2(diene) compounds, the similarity of the olefinic ^1H and ^{13}C NMR chemical shifts to those of free alkenes, and the absence of Pt−H or Pt−C couplings to the $=CH_2$ group clearly show that—unlike the PtR_2 compounds **1** and **2**—the terminal C=C bonds in the ω-alkenyl ligands are not coordinated to Pt. As seen in other Pt^{II} alkyls, there are long-range $^3J_{PtC}$ couplings[30,31] of ca. 30 Hz to the vinyl Si−CH= carbon in **1-COD**, the allylic Si-CH_2 carbon in **2-COD**, and to the Si-Me carbon atoms in both compounds.

Unlike their carbon analogues, $Pt(CH_2CMe_2CH{=}CH_2)_2(COD)$ and $Pt(CH_2CMe_2CH_2CH{=}CH_2)_2(COD)$, which readily release COD in solution and form the COD-free PtR_2 compounds,[18] **1-COD** and **2-COD** are stable in solution and very little (<5%) of the bound COD ligands are dissociated at room temperature. The higher binding strength of COD to **1** and **2** relative to their carbon analogues may be ascribed in part to the reduced steric size of unidentate CH_2SiR_3 vs CH_2CR_3 groups, although electronic factors such as the lower trans influence[16,32,33] of unidentate CH_2SiR_3 vs CH_2CR_3 groups may also play a role.

Like their COD analogues, the DBCOT compounds **1-DBCOT** and **2-DBCOT** show little dissociation of DBCOT in solution. In contrast, **1-NBD** partially dissociates in benzene-d_6 at room temperature to form **1** and NBD (Figure S3.17); this behavior is probably related to the higher air and thermal sensitivity of **1-NBD** compared to **1-COD**. The stability of **1-NBD** can be increased by adding excess NBD to disfavor the dissociation: a solution of **1-NBD** is indefinitely stable in air at −20 °C in the presence of 160 equiv of NBD. We will show later that this inhibition effect can be used to lengthen the latency period when these compounds are used as hydrosilylation catalysis.

The bonding strengths of these three dienes to the PtR_2 fragment can be assessed from their trans influence as deduced from the $^1J_{PtC}$ coupling constant for the α-CH_2 carbon of the ω-alkenyl groups (Table 2). This coupling constant, which increases in the order of **1-DBCOT** (694.9 Hz) < **1-COD** (704.9 Hz) < **1-NBD** (748.8 Hz), suggests that the Pt-diene bonding strength decreases in the same order, with the bonding of Pt to DBCOT being slightly stronger than to COD and much stronger than to NBD.

The dienes in the Si-allyl compounds **2-COD** and **2-DBCOT** are more prone to dissociate from Pt than are the dienes in the Si-vinyl counterparts compounds **1-COD** and **1-DBCOT**: when dissolved in benzene-d_6 solution, both **2-COD** and **2-DBCOT** slowly release diene to form observable (although small) amounts of **2** over several hours. This behavior is not due to weaker Pt-diene bonding in **2-COD** vs **1-COD** (the diene is equally strongly bonded in both complexes, as they are in the two DBCOT analogues). Instead, the behavior is consistent with the higher stability of **2** compared to **1** as a result of the smaller ring strain of the chelated ω-alkenyl ligand.

We will describe in a later section the rate at which COD dissociates from **1-COD** and **2-COD**.

Comparison of Hydrosilylation Activities of the PtR_2(COD) Compounds. To begin our hydrosilylation studies, we first compared the ability of three PtR_2(COD) compounds to catalyze the same two hydrosilylation reactions. The three compounds are

- $Pt(CH_2SiMe_2CH{=}CH_2)_2(COD)$ (**1-COD**)
- $Pt(CH_2SiMe_2CH_2CH{=}CH_2)_2(COD)$ (**2-COD**)
- $Pt(CH_2SiMe_3)_2(COD)$ (**3-COD**)

https://doi.org/10.1021/jacs.1c06846
J. Am. Chem. Soc. 2021, 143, 17492−17509

Table 4. Hydrosilylation of Different Olefin Substrates with MD′M Catalyzed by 1-COD[a]

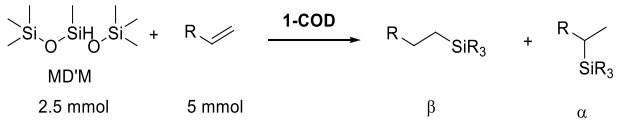

Entry No.	Mol olefin/ mol silane	Olefin substrate[a]	Cat. loading (10^{-6} mol%)	Temp (°C)	Conversion after reaction time of 30 min	4 h	24 h	selectivity
10	2	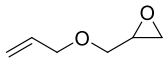	5	50	73%	>99%	>99%	5.9/1[c]
13	2	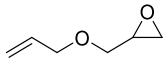	5	80	98%	>99%	>99%	7.7/1[c]
14	2	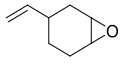	5	50	79%	>99%	>99%	>20/1[c]
15	2	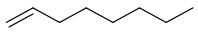	5	17	0 %	3%	11%	---
16	2	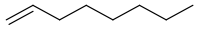	5	50	51%	95%	99%	>20:1[c]
17	2	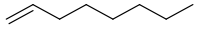	5	80	97%	>99%	>99%	>20:1[c]
18	2	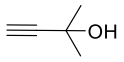	5	50	0%	0%	<2%	---
19	2	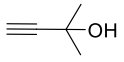	50	50	3%	12%	33%	2/1[b]
20	2	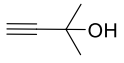	5	80	6%	24%	40%	2/1[b]
21	1	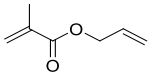	5	50	0%	24%	51%	1.4/1[d]
22	2	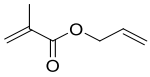	50	50	23%	97%	99%	1.4/1[d]
23	2	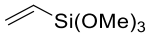	5	50	0%	12%	12%	7.5/1[b]
24	2	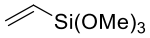	50	50	1%	69%	69%	7.3/1[b]
25	2	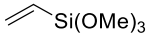	5	80	13%	73%	92%	7.5/1[b]
26	1	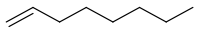	5	17	0.8%	7%	47%	>20:1[c]
27	1	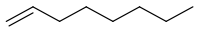	5	80	98%[e]	98%	-	>20/1[c]
28	1	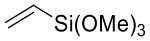	5	17	0	0.3%	0.5%	-
29	1	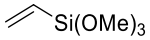	5	80	11%	78%	94%	7.9/1[b]
30	1	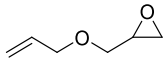	5	80	88%[e]	-	-	5.9/1[c]

[a]2 equiv of olefin per silane used unless otherwise specified. [b]Ratio of anti-Markovnikov to Markovnikov hydrosilylation product. [c]Ratio of anti-Markovnikov hydrosilylation product to internal olefin isomerization products; the Markovnikov hydrosilylation product is not formed (see text). [d]Ratio of anti-Markovnikov hydrosilylation product to the allyloxy silyldealkylation product 1,1,1,3,5,5,5-heptamethyltrisiloxan-3-yl methacrylate, which is generated along with propene; the Markovnikov hydrosilylation product is not formed (see text). [e]Full conversion of olefin starting material.

The compound **3-COD**[19] was chosen in order to determine whether the vinyl and allyl groups in **1-COD** and **2-COD** play an important role. We note here that platinum(II) akynyl compounds $Pt(C{\equiv}CR)_2(COD)$ have previously been reported to be active hydrosilylation precatalysts.[2]

All three compounds were assessed for their ability to catalyze the hydrosilylation of allyl glycidyl ether (AGE) with two silanes: $HSiEt_3$ and $HSiMe(OSiMe_3)_2$ (MD′M); these substrates were chosen for their industrial relevance. In a preliminary trial, 2 equiv of olefin were used unless otherwise

https://doi.org/10.1021/jacs.1c06846
J. Am. Chem. Soc. 2021, 143, 17492−17509

specified to ensure full conversion of the silane. Precatalyst loadings were 5×10^{-5} mol % Pt unless otherwise specified. The reactions were all conducted without solvent (i.e., neat).

The results are summarized in Table 3. At room temperature, all three precatalysts show essentially no activity after 1 h. At higher temperatures, however, **1-COD** and **2-COD** are highly active: the reaction of the silane with AGE to hydrosilylated products is complete within 2 h at 60 °C for $HSiEt_3$ and within 4 h at 50 °C for MD′M.

In contrast, **3-COD** is far less active: the conversion of $HSiEt_3$ to hydrosilylated products is only 12% complete after 2 h at 60 °C. This result shows that the Si-vinyl and Si-allyl groups in **1-COD** and **2-COD** facilitate the generation of the active catalyst, most likely by assisting in the dissociation of the COD ligands, which we know occurs in solution (see below).

Of these three compounds, **1-COD** has the longest latency under ambient conditions and is the most catalytically active at lower loadings: for hydrosilylation of AGE and MD′M at 50 °C and 5 ppm loadings, the conversion is 100% complete after 4 h for **1-COD** but only 10% complete for **2-COD**.

Substrate Scope for Hydrosilylation Catalysis by 1-COD. We find that **1-COD** catalyzes the hydrosilylation of a wide variety of olefins at moderate temperatures (50−80 °C), whereas very little catalysis occurs at room temperature over 4 h (Table 4); the standard conditions used were neat (no solvent), a precatalyst loading of 5×10^{-6} mol % (per Si−H bond), and 2 equiv of olefin per silane (to ensure full conversion of silane and minimize effects should isomerization of the olefin occur). A few reactions were also carried out with 1 equiv of olefin per silane to study the reaction behavior under conditions more likely to be employed commercially (Table 4).

With MD′M as the silane, the catalyst is active for the hydrosilylation of allyl glycidyl ether (AGE), vinylcyclohexene oxide (VCE), 1-octene, vinyltrimethoxysilane (VTMOS), and allyl methylmethacrylate (AMA). The reaction mixtures remain colorless even at full conversion. For a catalyst loading of 5×10^{-6} mol %, most of these olefins—AGE, VCE, and 1-octene—are extensively (~50%) hydrosilylated within 30 min at 50 °C, whereas for others—VTMOS and AMA—essentially no hydrosilylation occurs within the first 30 min at 50 °C, although the reaction accelerates at longer times or higher temperatures. In contrast, for the alkyne dimethyl ethynylcarbinol (DMEC),[1] the hydrosilylation yields are quite low even at higher catalyst loadings or higher temperatures, and the solutions tend to turn yellow. β-Alkynols such as DMEC are known inhibitors of platinum-based hydrosilylation catalysts, so much so that they can be considered as catalyst poisons.[34]

The high viscosity of oligomeric and polymeric samples does not significantly affect the reactivity of **1-COD**. When 5×10^{-5} mol % Pt (per Si−H) of **1-COD** is added to a 1:1 mixture of $CH_2{=}CHSiMe_2(OSiMe_2)_5SiMe_2CH{=}CH_2$ ($M^{Vi}D_5M^{Vi}$) and $HSiMe_2(OSiMe_2)_{100}SiMe_2H$ ($M'D_{100}M'$) at room temperature there is no sign of reaction after 24 h, and only 30% conversion of silane is observed after 7 days. When the mixture is heated to 80 °C, however, the hydrosilylation reaction goes to completion in 4 h. At full completion, there is no coloration due to colloidal Pt (Figure S8.4). The resulting polymer has a number-average molecular weight M_n of 146 kDa, a weight-average molecular weight M_w of 275 kDa, and a polydispersity index PDI of 1.88. This PDI is consistent with high (~90%) conversion of the monomers to polymer.[35]

Unlike the results typically seen for the industry-standard Karstedt's catalyst, olefin reduction products are nearly absent, and the anti-Markovnikov selectivity and yield of the hydrosilylation products seen for **1** are comparable to or better than those reported for Pt^0 NHC complexes,[10,11] and at much lower Pt loadings. The tendency of Karstedt's catalyst to form significant amounts of olefin isomerization and/or hydrogenation products is thought to be caused by multinuclear or colloidal platinum(0) species;[14] the small amounts of these products and the absence of coloration[10] suggest that formation of colloidal Pt species is disfavored in this $PtR_2(COD)$ system. For some olefins such as AGE that have allylic hydrogen atoms, only the anti-Markovnikov hydrosilylation product is formed; the Markovnikov product is not seen because the relevant platinum alkyl intermediate undergoes rapid β-H elimination instead,[9] so that the internal olefin is the only other product generated.[36] Overall, the isolated yields of anti-Markovnikov hydrosilylation products are comparable with the results from Pt^0 NHC complexes.[10,11]

Compared to reactions with 2 equiv of olefin per silane, using 1 equiv of olefin per silane (Table 4) results in much more hydrosilylation (i.e., a shorter latency period) at room temperature for 1-octene but little change the amount of hydrosilylation (i.e., an equally long latency period) for VTMOS. We will show below that we can take advantage of this different behavior to extend the latency period for olefins such as 1-octene that are rapidly hydrosilylated if 1 equiv per silane is used.

The ease of synthesis and use, the heat triggerable behavior, the high catalytic activity, and the good anti-Markovnikov selectivity of **1-COD** suggest that this compound would be useful for applications such as liquid injection molding and solvent-free hydrosilylation reactions.

Kinetics of Catalyst Activation and Hydrosilylation by 1-COD. To further understand the catalytic mechanism, we carried out a time-dependent study of the hydrosilylation of AGE and triethylsilane by **1-COD** at 60 °C with an olefin/silane/catalyst mole ratio of $2{:}1{:}2 \times 10^{-5}$. The reaction is characterized by an induction period during which the catalyst activates: less than 5% conversion of silane occurs after 20 min, but shortly thereafter the reaction accelerates quickly. The reaction rate reaches a maximum at 70 min, at which time 40% of the silane has been converted, then slows due to consumption of reactants. The reaction reaches >90% conversion of silane after 120 min. Overall, the curve describing the concentration of hydrosilylation products as a function of time has a sigmoidal shape (Figure 6). These results indicate that **1-COD** itself is not a hydrosilylation catalyst, but instead is a precatalyst that converts in some way into the active catalyst. In the next sections, we describe experiments to elucidate the catalyst activation mechanism.

Thermolysis of 1-COD in Solution in the Absence of Olefins and Silanes. The active species in Pt^{II}-catalyzed hydrosilylation reactions are believed to be molecular Pt^0 species, which convert into Pt^{II} silyl/hydride intermediates by non-rate-determining oxidative addition of silane.[9] The conversion of **1-COD** to a Pt^0 species could occur either (1) by thermal decomposition or (2) by reaction with silane.

To distinguish these possibilities, we heated a mixture of **1-COD** (2×10^{-3} mol % per silane) and olefin (2 equiv per silane) for 2 h at 75 °C (conditions under which the hydrosilylation reaction reaches competition if silane is present). The solution was then cooled to 20 °C; subsequent addition of silane and heating to 60 °C results in a catalytic rate that is identical to that seen without the preheating step. This finding, which is

https://doi.org/10.1021/jacs.1c06846
J. Am. Chem. Soc. 2021, 143, 17492−17509

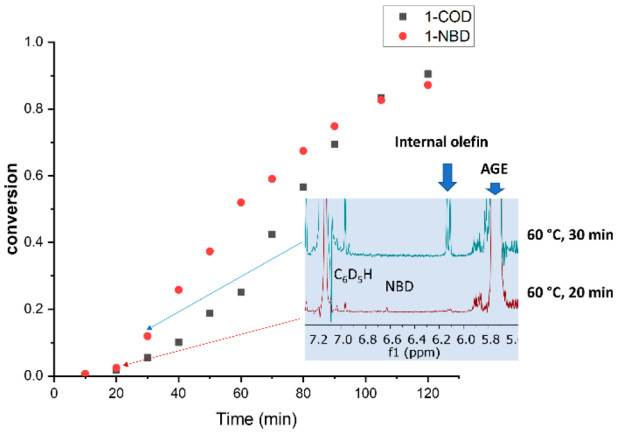

Figure 6. Reaction profile of the hydrosilylation of AGE with triethylsilane in the presence of catalyst (either **1-COD** or **1-NBD**) at a mole ratio of 2:1: 2×10^{-5} at 60 °C. For **1-NBD**, 160 equiv/Pt of NBD is also present at $t = 0$; the reaction takes off after the NBD is consumed.

consistent with TGA data that indicate that **1-COD** does not decompose thermally up to ∼100 °C (Figure S5.1), suggests that thermal decomposition of **1-COD** is not the principal mechanism by which catalyst activation occurs.

In order to confirm that catalyst activation does not occur by thermal decomposition of **1-COD**, we also studied the thermolysis of the COD-free analogue **1** and that of the related compounds **2** and **4**. In the next sections, we describe these studies and then compare these thermolysis rates with the rate of reaction of **1-COD** and **1** with silanes. This latter comparison gives useful insights into how **1-COD** coverts into the active catalyst.

Thermolysis of the PtR_2 Compounds 1 and 2 in the Absence of Silanes. Formation of the New Compound $Pt(CH_2SiMe_2CH_2SiMe_2CH{=}CH_2)_2$ (4). The behavior of the vinyl-Si compound **1** at higher temperatures was studied in C_6D_6; a drop of Hg was added to minimize side reactions caused by the formation of colloidal Pt.[37] When the solutions are heated to 50 °C, ∼ 80% of **1** decomposes in 4 h. Thermolysis at lower concentrations (0.01 M) follows first-order kinetics with a rate constant of 6.6×10^{-3} min^{-1}, whereas thermolysis at higher concentrations (0.08 M) deviates from first order kinetics (Figure S5. 4).

Several thermolysis products can be identified: the major ones are vinyltrimethylsilane (formed by adding a hydrogen atom to one of the ligands in **1**) and several compounds having SiR_3-CH_2−SiR_3 backbones; small amounts of ethylene and other light olefins are also formed (Scheme 3):

To determine the fate of the platinum atoms, we also carried out studies of the thermolysis of **1** in the presence of excess diphenylacetylene (DPA), a hydrosilylation substrate that can also trap molecular Pt^0 species in the form of a stable complex, $Pt(DPA)_2$.[38] Thermolyses conducted at 50 °C at two different concentrations of **1** (0.008 and 0.08 M) both follow first-order decay, with a rate constant of $7(2) \times 10^{-3}$ min^{-1} (Figure S5.4) that is very similar to the rate constant seen for the thermolysis of **1** at low concentration in the absence of DPA. A ^1H NMR resonance at ∼ δ 7.8 (Figure 7) shows that 66% of **1** is trapped as the molecular Pt^0 species of $Pt(DPA)_2$.[38]

In addition to $Pt(DPA)_2$, thermolysis of **1** in the presence of DPA generates the same organic products seen in the absence of DPA (Scheme 4 and Figure 7), along with a small amount (15%

Scheme 3. Products of the Thermolysis of 1 in C_6D_6[a]

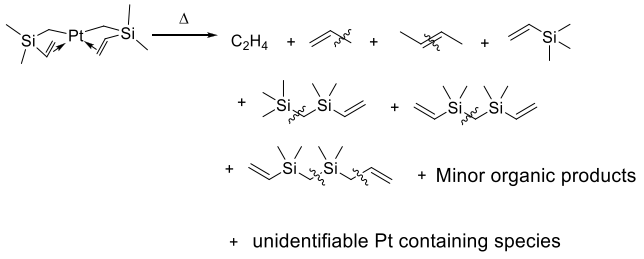

[a]Wavy lines indicate bonds that are formed from fragments generated by cleavage of Si−C bonds in **1**. Quantifying the amounts of these products is affected by evaporative losses and by peak overlaps in the NMR spectra.

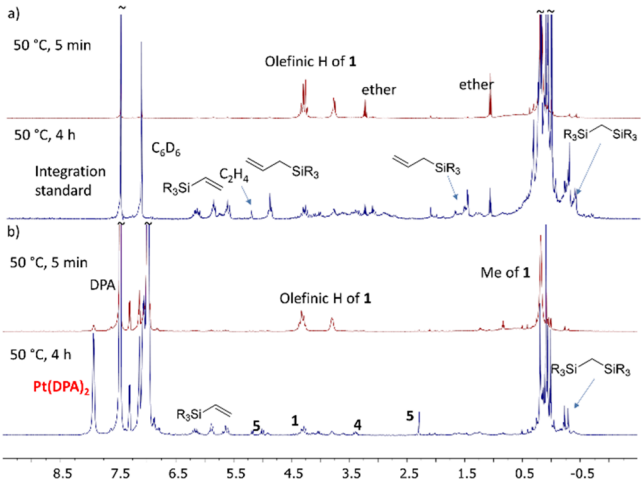

Figure 7. (a) ^1H NMR spectra in C_6D_6 at 50 °C of **1** (upper) and its thermolysis products (lower); 1,4-bis(trimethylsilyl)benzene is present as an integration standard. (b) ^1H NMR spectra in C_6D_6 at 50 °C of **1** (upper) and its thermolysis products (lower) in the presence of excess DPA to trap the generated Pt^0 species. Additional characterization of the thermolysis products (GC−MS spectra, 2D NMR spectra, and isolation of **4** and **5**) are included in the Supporting Information.

Scheme 4. Products of the Thermolysis of 1 in C_6D_6 in the Presence of Diphenylacetylene[a]

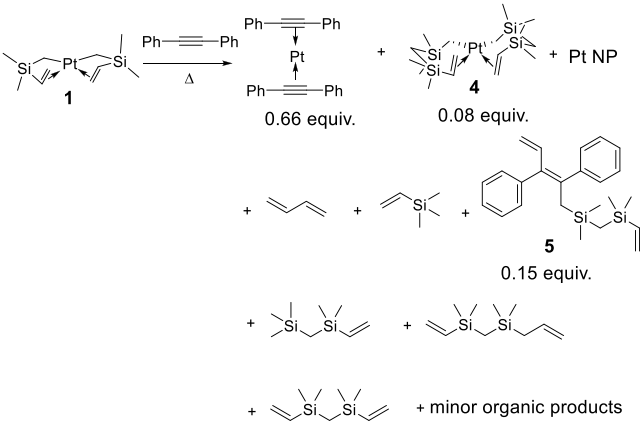

[a]Wavy lines indicate bonds that are formed from fragments generated by cleavage of Si−C bonds in **1**. Quantifying the amounts of these products is affected by evaporative losses and by peak overlaps in the NMR spectra.

https://doi.org/10.1021/jacs.1c06846
J. Am. Chem. Soc. 2021, 143, 17492−17509

of **1** decomposed) of a DPA derivative (**5**), which can be viewed as the result of insertion of DPA into the fragments generated from the ligands in **1**.

Interestingly, during thermolysis either in the presence or absence of DPA, about 8% of **1** is converted into a new air- and water-stable platinum-containing product, Pt-$(CH_2SiMe_2CH_2SiMe_2CH{=}CH_2)_2$ (**4**), which we have characterized crystallographically (Figure 8). No other molecular

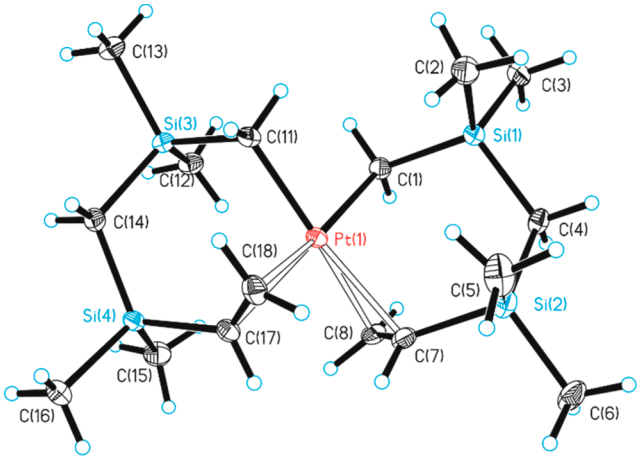

Figure 8. Crystal structure of $Pt(CH_2SiMe_2CH_2SiMe_2CH{=}CH_2)_2$ (**4**). Ellipsoids are drawn at the 35% probability level.

platinum species can be identified in the NMR spectrum. Presumably, the remaining 25% of **1** is converted to Pt nanoparticles and causes the yellow color of the solution.

These results strongly suggest that thermolysis of **1** yields Pt^0 species, and also that the deviation from first-order kinetics seen for thermolysis of **1** at higher concentrations in the absence of DPA is due to a bimolecular process promoted by free Pt^0. Furthermore, the product distribution suggests that a major pathway in the decomposition of **1** is likely β-carbon transfer,[24,39] in which a Si−vinyl bond breaks to form an intermediate containing coordinated silene ($CH_2{=}SiMe_2$) and vinyl groups (Scheme 5). Compound **4**, for example, is the result

Scheme 5. Possible Mechanism for the Formation of Two of the Thermolysis Products Generated from 1

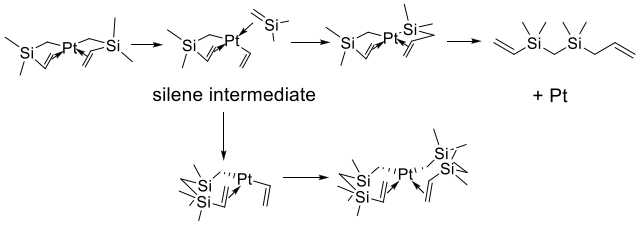

of inserting $CH_2{=}SiMe_2$ fragments into each of the two the Pt−C bonds in **1**, and the formation of the allylic disila-alkane product $CH_2{=}CHSiMe_2CH_2SiMe_2CH_2CH{=}CH_2$ can be explained by a similar mechanism:[1,9,40]

For the Si-allyl compound **2**, the thermolysis appears to follow autocatalytic kinetics (see Figure S5.35). The ^1H NMR spectrum and GC-MS analysis show the formation of large amounts of propylene, allylplatinum species, and a mixture of organosilanes and organodisilanes (see Figures S5.34-S5.41). The formation of these products is consistent with cleavage of the Si−allyl bond to generate an allyl/silene intermediate. Such a bond cleavage process is consistent with the shortening of Si−C_α bond seen in the crystal structure of **2**, although activation of Si−allyl bonds by intermolecular processes[41] cannot be ruled out.

We conclude from the results in this section that (in the absence of silane) **1** converts efficiently to a Karstedt-like molecular Pt^0 species over several hours when it is heated to 60 °C. In order to determine exactly how **1-COD** converts to active Pt^0 species under catalytic conditions, we need to compare this rate to the rate at which **1** reacts with silane, and determine two other kinetic terms: the rate at which **1-COD** loses **COD** to form **1**, and the rate at which **1-COD** and **1** react with silanes. We will discuss the second of these kinetic terms first.

Reactions of the PtR_2 and PtR_2(COD) Compounds with Silanes. To determine the rate at which the platinum compounds react with silanes, we treated a solution of **1** in benzene-d_6 with 3 equiv of the silane $SiHMe(OSiMe_3)_2$ (MD′M) in the presence of an excess of the Pt^0 trapping agent (and hydrosilylation substrate) diphenylacetylene (DPA) at 20 °C. This reaction is very fast: **1** is converted nearly quantitatively into $Pt(DPA)_2$ within 5 min. The organic byproducts (Figure 9) consist of vinyltrimethylsilane, (H−

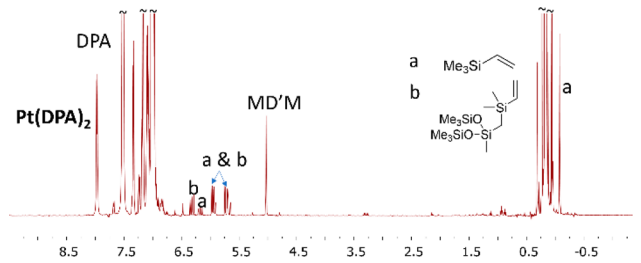

Figure 9. ^1H NMR spectrum in C_6D_6 at 20 °C of the reaction of **1** with MD′M in the presence of a large excess of diphenylacetylene (DPA). All **1** reacted within 5 min to generate $Pt(DPA)_2$, vinyltrimethylsilane (H−$CH_2SiMe_2CH{=}CH_2$, species a), and 3-((dimethyl(vinyl)silyl)-methyl)-1,1,1,3,5,5,5-heptamethyltrisiloxane ($R_3Si{-}CH_2SiMe_2CH{=}CH_2$, species b).

$CH_2SiMe_2CH{=}CH_2$, 3-(dimethyl(vinyl)silylmethyl)-1,1,1,3,5,5,5-heptamethyltrisiloxane, $(Me_3SiO)_2MeSi{-}CH_2SiMe_2CH{=}CH_2$, and the hydrosilylation products of these two vinylsilanes. The two vinylsilane products can be viewed as being generated by the addition of an H atom or a $SiMe(OSiMe_3)_2$ group from MD′M, respectively, to the $CH_2SiMe_2CH{=}CH_2$ ligands of **1**. Similar products were seen upon treatment of **2** with MD′M under the same conditions: PtL_2 is rapidly converted to $Pt(DPA)_2$, L-H, and L-SiR_3 within minutes, where L = $CH_2SiMe_2CH_2CH{=}CH_2$ (Scheme 6).

The much faster rates for the reaction of **1** or **2** with silane compared to the rates of thermolysis clearly show that the conversion of **1** or **2** into active catalyst is caused by reaction with silane. The principal organic products, L−H and L−SiR_3, where L is the ω-alkenyl group in **1** and **2**, suggest that the silane adds oxidatively to the PtL_2 species (or undergoes σ-complex-assisted metathesis[42]), after which the ligands L eliminate as L−H and L−SiR_3 to form the active catalyst. Oxidative addition of a silane to a Pt^{II} alkyl complex to form a Pt^{IV} product is known;[43] a similar reaction has previously been reported to be the catalyst activation mechanism for $Pt(COD)(C{\equiv}CR)_2$ complexes,[2] and may also be operative here.

Addition of MD′M to the COD adducts **1-COD** and **2-COD** at 20 °C in the presence of excess diphenylacetylene also

https://doi.org/10.1021/jacs.1c06846
J. Am. Chem. Soc. 2021, 143, 17492−17509

Scheme 6. Products from the Reaction of PtR_2 Complexes 1 and 2 with MD′M in the Presence of Excess Diphenylacetylene (DPA)[a]

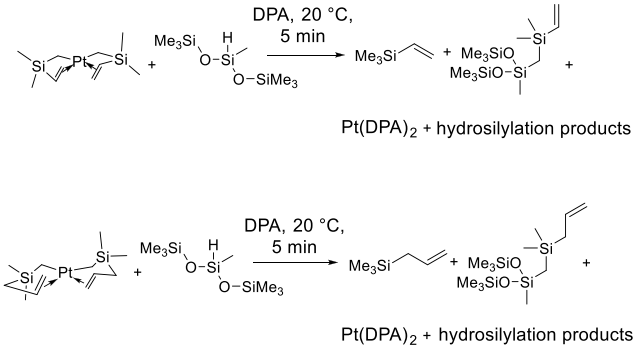

[a]Quantifying the amounts of these products is affected by evaporative losses and by secondary hydrosilylation reactions.

generates 1 equiv each of $Pt(DPA)_2$, COD, L-H, and L-SiR_3 (Figure 10, Scheme 7 and Figure S6.18). These rates are much

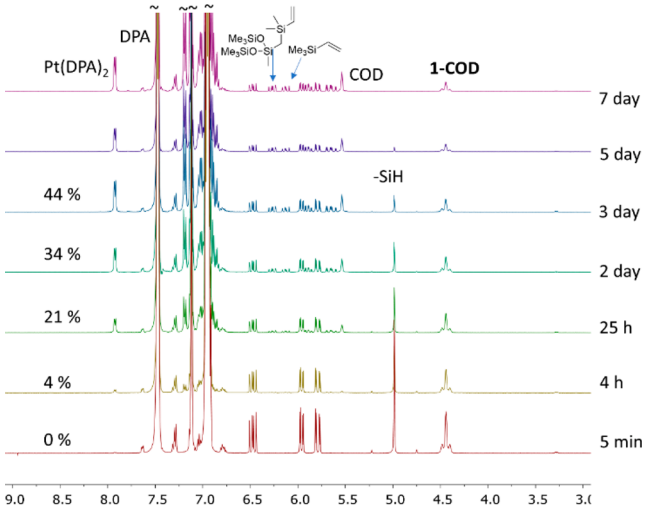

Figure 10. ^1H NMR spectra in C_6D_6 at 20 °C of the reaction of **1-COD** with excess MD′M in the presence of a large excess of diphenylacetylene (DPA); the reaction products are $Pt(DPA)_2$, vinyltrimethylsilane (H–L), 3-((dimethyl(vinyl)silyl)methyl)-1,1,1,3,5,5,5-heptamethyltrisiloxane (R_3Si–L), and COD. The percentage conversion of **1-COD** to $Pt(DPA)_2$ (given at the left of the figure) matches well with the kinetics of COD dissociation from **1-COD**. After 3 days of reaction, the majority of MD′M was consumed by hydrosilylation of diphenylacetylene instead of reacting with **1-COD**.

slower than the rate of reaction of **1** with silane, but are consistent with the hydrosilylation rates seen for these COD adducts at room temperature. For example, for **1-COD**, the yield of $Pt(DPA)_2$ is too small to be measured after 10 min, only 4% after 4 h, and 43% after 3 days. The reaction of MD′M with **2-COD** is similarly slow at 20 °C.[44]

Kinetics of COD Dissociation. The results above suggest that the rate-determining step for the catalysis is the loss of COD from **1-COD** to generate **1**, which then reacts rapidly with silane to form catalytically active molecular Pt^0 species. This suggestion is also consistent with the finding that **1-COD** is a better precatalyst for hydrosilylation than the trimethylsilyl compound **3-COD**: as we concluded above, the Si-vinyl groups

Scheme 7. Products from the Reactions of 1-COD and 2-COD with MD′M in the Presence of Excess Diphenylacetylene (DPA)

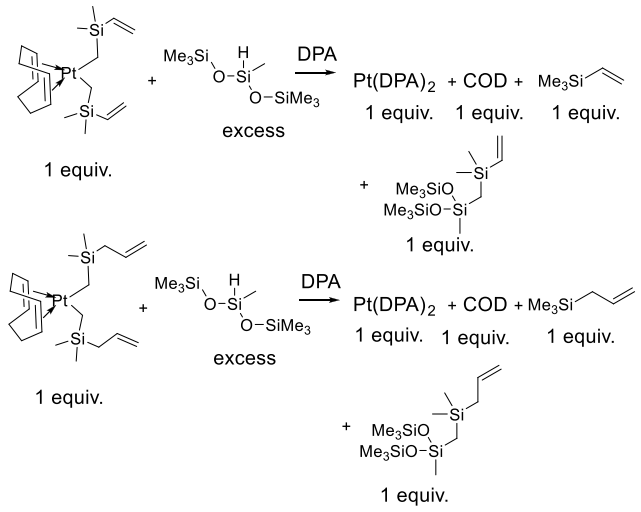

in **1-COD** (and the Si-allyl groups in **2-COD**) facilitate the generation of the active catalyst, most likely by assisting in the dissociation of the COD ligands.

To better understand the COD dissociation process, we investigated the ligand substitution reaction between **1-COD** and dibenzo[*a*,*e*]cyclooctatetraene, DBCOT. We find that, at 80 °C, the reaction between **1-COD** and 2 equiv of DBCOT to form **1-DBCOT** and COD reaches equilibrium within 15 min; the equilibrium constant for this exchange reaction is 1.3. The measured equilibrium constant is consistent with the conclusions from the $^1J_{PtC}$ coupling constants to the α-CH_2 carbon of the ω-alkenyl groups, which suggested that the bonding of Pt to DBCOT was slightly stronger than to COD.

To show that the ligand exchange between **1-COD** and DBCOT is indeed initiated by dissociation of COD (not association of DBCOT), we studied the rate of conversion from **1-COD** to **1-DBCOT** as a function of the concentration of DBCOT. For quantitative measurements of the rate of the dissociation of the COD ligand in **1-COD**, 20 equiv of DBCOT was added, so the concentration of **1-COD**, which under these circumstances decreases to a very small value at final equilibrium, could be fitted at early times to a decaying exponential; the derived rate constant is that for displacement of COD from **1-COD**. At 60 °C in benzene-d_6, the first order rate constant is independent of the concentration of DBCOT (Figure 11); this result clearly shows that the exchange mechanism does not involve association of DBCOT; thus, the rate for generation of **1-DBCOT** from **1-COD** is the rate of dissociation of COD from **1-COD**.

Measurements taken at four different temperatures between 39.7 and 69.7 °C were fitted to the Eyring equation to give $\Delta H^{\ddagger}$ = 21 ± 1 kcal mol^{-1} and $\Delta S^{\ddagger}$ = −12 ± 4 cal mol^{-1} K^{-1}. The negative entropy of activation implies that the transition state for the exchange reaction is more ordered than the ground state structure of **1-COD**. We suggest that, in the transition state for dissociation of COD, the C═C bonds of one or both of the ω-alkenyl ligands (begin to) coordinate to Pt (Scheme 8).

The measured rate constant for COD dissociation matches well with the kinetics for catalyst activation. Extrapolating the Eyring plot to lower temperatures gives a rate constant of 2.9 × 10^{-6} s^{-1} at 20 °C, which corresponds to a 4% conversion in 4 h,

https://doi.org/10.1021/jacs.1c06846
J. Am. Chem. Soc. 2021, 143, 17492−17509

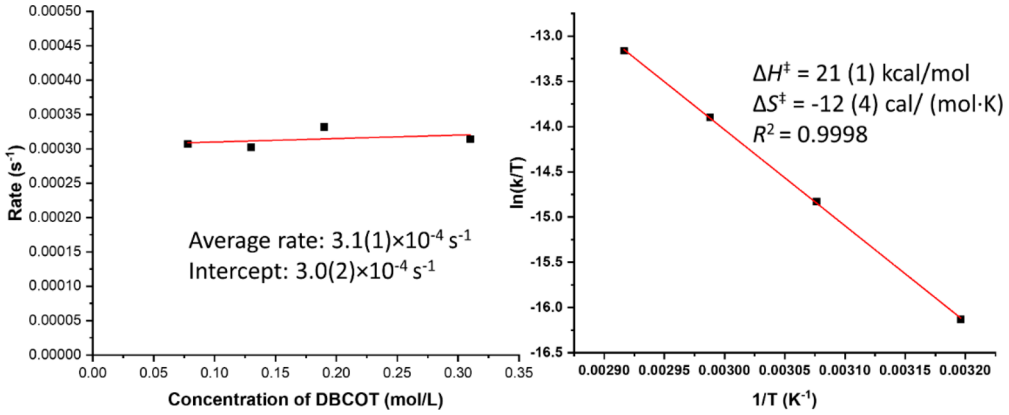

Figure 11. (Left) Rate of the ligand-exchange reaction between **1-COD** and DBCOT in benzene-d_6 as a function of the concentration of DBCOT at 62 °C. The ligand exchange rate is independent of the concentration of DBCOT, suggesting a dissociative mechanism. (Right) Eyring plot for the ligand exchange reaction between **1-COD** and DBCOT in benzene-d_6. The negative entropy of activation suggests that internal association of the ω-alkenyl ligands leads to the dissociation of COD.

Scheme 8. Possible Mechanism for COD Dissociation in 1-COD

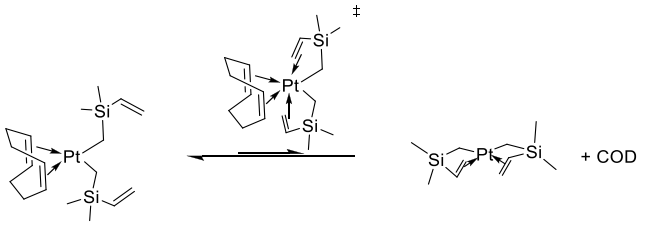

23% conversion in 25 h, and a $t_{1/2}$ of ~3 days. These numbers match well with those observed for the reaction between **1-COD** and MD′M, for which the conversion percentages after 4 h, 25 h, and 3 days were 4%, 21%, and 44%, respectively (Figure 10). We also calculate that the $t_{1/2}$ is approximately 7 min at 80 °C. This value also matches well with the observed fast initiation of the hydrosilylation reaction at this temperature.

The COD-DBCOT exchange rate for **2-COD** is somewhat slower (Table 5), which is consistent with its slower rate of

Table 5. Rate of Substitution of COD in 1-COD and 2-COD with DBCOD

T (°C)	exchange rate (**1-COD**) (s^{-1})	exchange rate (**2-COD**) (s^{-1})
69.7	6.6×10^{-4}	4.1×10^{-4}
61.5	3.1×10^{-4}	1.6×10^{-4}
51.9	1.2×10^{-4}	5.2×10^{-5}
39.7	3.1×10^{-5}	1.4×10^{-5}

catalyst activation when heated. Fitting the COD-DBCOT exchange rate to the Eyring equation gives $\Delta H^{\ddagger} = 23 \pm 2$ kcal mol^{-1} and $\Delta S^{\ddagger} = -6 \pm 5$ cal mol^{-1}·K^{-1} (see Figure S7.5).

Mechanism and Rate Law of Catalyst Activation. The above results show that **1-COD** converts to a catalytically active molecular Pt^0 species by a three-step process: (1) Slow dissociation of the bound COD ligand from **1-COD** to generate the Pt^{II} ω-alkenyl intermediate **1**. This step is rate determining and is assisted by coordination of the C═C bonds of the ω-alkenyl ligand to Pt. (2) Fast reaction of silane with the Pt^{II} ω-alkenyl intermediate **1** (e.g., by oxidative addition to form a Pt^{IV} silyl/hydride intermediate or by σ-complex-assisted metathesis, Scheme 9). (3) Fast elimination of L-H and L-SiR_3 to form a

Scheme 9. Proposed Mechanism for Conversion of 1-COD to Pt^0

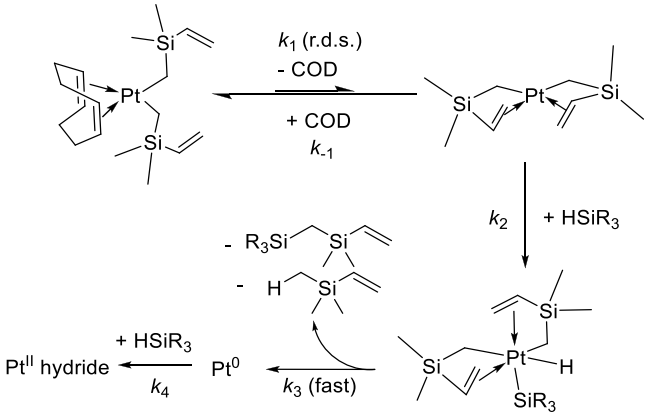

molecular Pt^0 species (where L is the ω-alkenyl ligand). Steps 2 and step 3 are highly efficient and lead to near-quantitative conversion of **1** to Pt^0 species.

The net result of these steps is formation of a Karstedt-like Pt^0 species. As has been determined in other systems,[9] the molecular Pt^0 species rapidly reacts with silane to afford a Pt^{II} hydride species, which is a key species in the catalytic cycle. The exact resting state of Pt following the generation of the Pt^0 species will depend on the nature of the substrate.[9]

Based on the above mechanism, we can derive a rate law for catalyst activation, i.e., the conversion of **1-COD** (or **2-COD**) to catalytically active Pt^0 species. We assume that the interconversion between **1-COD** and **1** is characterized by forward and backward rate constants of k_1 and k_{-1}, that the reaction of **1** with silane is irreversible and characterized by a rate constant of k_2, and that subsequent steps are fast (Scheme 9). We know that both association of COD and reaction of **1** with silane are fast. Applying a steady-state approximation to the Pt^{II} ω-alkenyl intermediate **1** (which we know from our NMR studies is present only in small amounts in solutions of **1-COD**), we can derive the following rate law for catalyst activation:

$$\text{rate} = k_1 k_2[\text{HSiR}_3][\textbf{1-COD}]/(k_{-1}[\text{COD}] + k_2[\text{HSiR}_3])$$

This rate law suggests that, for a selected concentration of precatalyst and silane, the rate of catalyst activation can be tuned by replacing the coordinated COD or ω-alkenyl ligands with

https://doi.org/10.1021/jacs.1c06846
J. Am. Chem. Soc. 2021, 143, 17492−17509

Table 6. Hydrosilylation of 1-Octene with MD′M (1 equiv) Catalyzed by 1-COD (5×10^{-6} mol %) with 0.1 mol % of an Added Inhibitor*

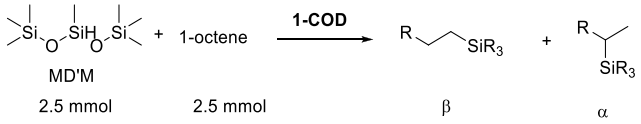

Inhibitor added	Temp (°C)	β/α ratio	Conversion after reaction time of 30 min	4 h	24 h	RT for 24 h, then at 80 °C
none	17	>20:1[a]	0.8%	7%	47%	88% in 30 min
none	80	>20:1[a]	98%	-	-	-
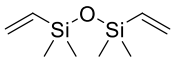	17	-	0%	0%	4%	85% in 30 min
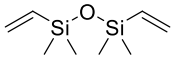	80	>20:1[a]	93%	-	-	-
NBD	17	>20:1[a]	0%	0%	37%	88% in 30 min
NBD	80	>20:1[a]	98%	-	-	-

*The inhibitors increase the latency at room temperature without otherwise affecting the catalysis. [a]Ratio of anti-Markovnikov hydrosilylation product to internal olefin isomerization products; the Markovnikov hydrosilylation product is not formed.

other dienes or chelating groups (which would change k_1 and k_{-1}). Addition of excess COD or other dienes may also inhibit the reaction of **1** with silane either by reducing the concentration of **1** in solution (which would affect the steps corresponding to k_{-1} and k_2) or by trapping the formed Pt^0 species (which would affect the step corresponding to k_4). Furthermore, one can also use existing strategies (often used for Karstedt's catalyst) to add an inhibitor that slows the conversion of the Pt^0 species to a Pt^{II} hydride (which would also affect the step corresponding to k_4).[1]

Significantly, even a small concentration of an inhibitor will have a great effect in the present design because the target of the inhibitor is only a small fraction of the metal centers (either **1** or the small amount of Pt^0 generated in the early stages of the catalysis) instead of the entire catalyst charge. In addition, if the added inhibitor can be consumed by being converted to a noninhibiting form (for example by hydrosilylation or hydrogenation[13]), as the concentration of the inhibitor decreases, the conversion of precatalyst to active catalyst will become less inhibited over time. Consequently, the rate of catalyst activation will accelerate as the reaction proceeds; the catalysis will therefore show autoinductive character. We explore these possibilities in the next sections.

Influence of Changing the Diene on Precatalyst Activation: Hydrosilylation Activity of 1-NBD. Our studies in solution (described above) showed that **1-NBD** partially dissociates in benzene-d_6 at room temperature to form **1** and NBD; in other words, NBD binds much more weakly than COD to Pt. As a result, **1-NBD** should convert to active catalyst more quickly than **1-COD**. As described above, **1-NBD**, as a pure material, is not particularly suited as a hydrosilylation catalyst because it rapidly decomposes at room temperature. We find, however, that we can greatly increase its thermal stability by adding excess NBD: under these conditions, **1-NBD** is stable for months, particularly if it is kept at −20 °C. This behavior is undoubtedly a Le Chatelier effect, in which the presence of excess NBD suppresses the formation of **1** from **1-NBD**.

We then carried out an investigation of the activity of **1-NBD** in the presence of excess NBD for the hydrosilylation of AGE and triethylsilane at 60 °C. The AGE/silane/catalyst mole ratio was $2{:}1{:}2 \times 10^{-5}$, and 160 equiv/Pt of NBD was present at $t = 0$. We find that, under these conditions, there is a 20 min induction period during which time little hydrosilylation of AGE takes place. However, during this period, the concentration free NBD is falling (Figure 6) because it is being hydrosilylated.[9] Notably, when the excess NBD disappears from the solution, the induction period ends and the reaction of AGE with triethylsilane begins to accelerate quickly. The overall result is that distinctly sigmoidal reaction kinetics are observed (Figure 6). Thus, the effect of adding NBD is to lengthen the latency period for catalyst activation through an autoinductive mechanism.

Relative to catalysis by **1-COD**, the catalytic rate accelerates more quickly for **1-NBD** after the induction period ends. This difference arises because (1) NBD binds more weakly than COD to Pt and (2) NBD can be consumed by hydrosilylation as a result of its higher ring strain. We will show in the next section that, in contrast, COD remains largely intact under these

https://doi.org/10.1021/jacs.1c06846
J. Am. Chem. Soc. 2021, 143, 17492−17509

reaction conditions, so that the kinetics of hydrosilylation using **1-COD** as the precatalyst is not autoinductive.[9]

Fate of COD during Hydrosilylation. Two pieces of evidence suggest that the majority of the free COD (which is generated as **1-COD** converts to active catalyst) remains intact during the hydrosilylation catalysis. First, at 20 °C, the reaction between **1-COD** and MD′M in the presence of diphenylacetylene generates one equiv of COD per equiv of $Pt(DPA)_2$ formed. No hydrogenation or isomerization of COD is observed. Second, heating a mixture containing MD′M (2 equiv), AGE (1 equiv), COD (1 equiv), and **1-COD** (5×10^{-5} mol %) at 100 °C leads to full conversion of AGE to hydrosilylation (or isomerization) products, whereas only 40% of the COD is hydrogenated to form cyclooctene. We conclude that the rate of COD consumption is likely slow compared to the rate of hydrosilylation and catalyst activation.

The reason that COD does not undergo hydrosilylation can be understood as follows: although COD can insert into metal−hydrogen bonds, such an insertion step is usually followed by regeneration of COD because β-hydrogen elimination to regenerate COD is rapid.[9]

Inhibition of Conversion of 1-COD to Active Catalyst by Addition of Consumable Dienes. An important observation is that catalytic hydrosilylation by **1-COD** is inhibited by addition of COD. The above mixture containing MD′M (2 equiv), AGE (1 equiv), COD (1 equiv), and **1-COD** (5×10^{-5} mol %) does not show any hydrosilylation of AGE over 24 h at 50 °C, whereas complete hydrosilylation occurs within 30 min under similar conditions if no free COD is added. The inhibition effect may be a consequence of either or both of the following effects: reducing the concentration of free **1** by shifting the equilibrium in favor of **1-COD**, or trapping the active Pt^0 catalyst as $Pt(COD)_2$. In either case, as the amount of added COD increases, the inhibition effect increases also.

COD has the effect of slowing the catalysis more or less permanently because COD is largely unreactive under the hydrosilylation conditions, as we showed in the previous section. An interesting question is whether we can slow the catalysis only temporarily, i.e., to increase the latency period of the hydrosilylation, by using a different inhibitor that is consumed over time. We propose that one strategy for increasing the latency period is to add small amounts of a free diene that can itself be hydrosilylated. It is likely that such a "consumable inhibitor" can function either by stabilizing **1** and inhibiting its reaction with silane, or by stabilizing the Pt^0 intermediate and inhibiting its reaction with silane. In either case, because the concentrations of **1** and Pt^0 are negligible at the beginning of the reaction, compared to the concentration of Pt^0 in catalytic reactions that employ Karstedt's catalyst, only a very small amount of a consumable inhibitor should be needed to increase the latency period. Eventually, however, as the inhibitor is converted into a different chemical form by being hydrosilylated, the inhibition effect will diminish; when the concentration of the consumable inhibitor approaches zero, the latency period will end.

We tested NBD and a vinyl silicate ester, 1,3-divinyl-1,1,3,3-tetramethyldisiloxane (DVTMS), as consumable inhibitors. Indeed, with a 1:1 ratio of olefin to silane and 5×10^{-6} mol % **1-COD** as a precatalyst, the latency seen for 1-octene increases from <0.5 h to >4 h at room temperature when 0.1 mol % per silane of NBD is added as a consumable inhibitor (Table 6). Even longer latency is seen when 0.1 mol % per silane of DVTMS is added.

Mechanism and Rate Laws for Hydrosilylation after the Catalyst Is Activated: The Role of Soluble Inhibitors. It is well-known that certain compounds can inhibit hydrosilylation by Karstedt's catalyst, most likely by binding to Pt^0 and poisoning its reactivity. Goddard et al. have previously suggested that the inhibitors commonly used in industrial hydrosilylation processes are not soluble in the reaction medium and that the inhibition is heterogeneous.[34] In our case, however, the consumable inhibitors we employ are clearly soluble in the reaction medium, so we can rule out this possibility. In addition, unlike NBD, DVTMS does not bind strongly to the Pt^{II} centers in **1**, so it is unlikely that it inhibits the conversion of **1** to Pt^0. Instead, we suggest that DVTMS inhibits the oxidative addition of silane to Pt^0 to form the Pt^{II} hydride intermediate. In the next paragraphs, we show how this hypothesis can explain a number of facts.

In a recent paper, Kühn et al. measured the rate laws for the hydrosilylation of norbornene and of 1-octene with trichlorosilane; in both reactions, the catalyst was Karstedt's catalyst.[9] Interestingly, for the hydrosilylation of norbornene, the rate law was $r = k_{obs}[Pt][HSiR_3]$: first order in catalyst, first order in silane, and zeroth order in olefin. For the hydrosilylation of 1-octene, the rate law was $r = k_{obs}[Pt][HSiR_3]^2/[olefin]$: first order in catalyst, second order in silane, and inverse first order in olefin. In addition, Kühn showed that norbornene binds much more strongly than 1-octene to Pt^0: the equilibrium constants for binding differ by about a factor of 10^5. Kühn proposed, correctly, we believe, that the different rate laws for the two olefins must reflect the different coordinating abilities of the olefin substrates. However, we wish to modify Kühn's mechanistic explanation of these two rate laws.

We agree with Kühn and others that the mechanism of hydrosilylation begins with a Pt^0−olefin complex B (using Kühn's lettering system), which reacts with silane to generate the Pt^{II} silyl/hydride species C (Scheme 10). Kühn also suggested that the rate-determining step (r.d.s.) of hydrosilylation is the subsequent migratory insertion of a bound olefin into the Pt−H bond of C to give the platinum alkyl species D.[9]

Here, we make use of theoretical support for Chalk and Harrod's original proposal that this migratory insertion step occurs via a five-coordinate platinum intermediate.[34] Thus, we

Scheme 10. Proposed Mechanism for Pt-Catalyzed Hydrosilylation

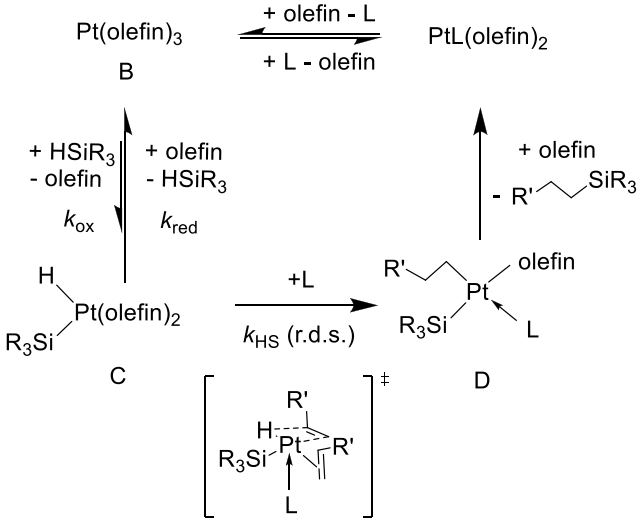

https://doi.org/10.1021/jacs.1c06846
J. Am. Chem. Soc. 2021, 143, 17492−17509

assume that the rate-determining step is the reaction of four-coordinate C with a species L and that migratory insertion of olefin into the Pt−H bond occurs in the resulting 5-coordinate intermediate. We furthermore assume that in some cases L is the olefin but in other cases (i.e., for more weakly binding olefins) L is the silane.[45] In the following paragraphs, we show how this latter assumption allows us to derive the rate laws found by Kühn for strongly and weakly binding olefins.

In the presence of nearly equal amounts of olefin and silane, the pre-equilibrium between B and C will most likely favor the olefin complex B (which is the resting state in the catalytic cycle), so that the concentration of B equals the catalyst loading [Pt], and species C will be present in very small amounts. If we apply the steady state assumption to intermediate C, we have

$$[C] = k_{ox}[Pt][HSiR_3]/(k_{red}[olefin] + k_{HS}[L])$$

where k_{ox} and k_{red} are the rate constants for oxidative addition and reductive elimination of silane and k_{HS} is the rate constant for the L-induced migratory insertion of olefin into the Pt−H bond. The overall rate of reaction is then given by the following equation:

$$r = k_{HS}[L][C] = k_{HS}k_{ox}[Pt][HSiR_3][L]/(k_{red}[olefin] + k_{HS}[L]) \quad (1)$$

For olefins that coordinate strongly to Pt^{II} (such as norbornene), the ligand L is likely to be the olefin. Replacing [L] with [olefin] in eq 1, we have

$$r = k_{HS}k_{ox}[Pt][HSiR_3][olefin]/(k_{red}[olefin] + k_{HS}[olefin])$$
$$= k_{HS}k_{ox}[Pt][HSiR_3]/(k_{red} + k_{HS})$$

This rate law shows that, for olefins that coordinate strongly to Pt^{II}, the reaction is first order in catalyst, first order in silane, and zeroth order in olefin, as reported by Kühn.

For olefins that bind weakly to Pt^{II} (such as 1-octene), the silane is more likely to coordinate to the Pt^{II} species C. In this case, we replace L with [$HSiR_3$] in eq 1. Therefore:

$$r = k_{HS}k_{ox}[Pt][HSiR_3]^2/(k_{red}[olefin] + k_{HS}[HSiR_3])$$

In this case, however, we can further simplify the rate law by realizing that $k_{HS}[HSiR_3] \ll k_{red}[olefin]$; this is true because the migratory insertion step (C to D) is rate determining and therefore slow. Then we obtain

$$r = k_{HS}K[Pt][HSiR_3]^2/[olefin]$$

where $K = k_{ox}/k_{red}$. In this case, as reported by Kühn, the reaction is first order in catalyst, second order in silane, and inverse first order in olefin. Note, however, that this mechanism does not necessarily mean that species D is a Pt^{IV} complex; it would be sufficient for the silane to bind to platinum to form a Pt^{II} sigma complex.

For a solution initially containing equal concentrations of the olefin and silane substrates (let us call this concentration S_0), the rate laws above for strongly and weakly binding olefins both reduce to the same form

$$r = k[Pt][HSiR_3] = k[Pt][olefin] = kS_0[Pt]$$

in which $k = k_{HS}k_{ox}/(k_{red} + k_{HS})$ for an olefin that coordinates strongly to Pt^{II}, whereas $k = k_{HS}k_{ox}/k_{red}$ for an olefin that coordinates weakly to Pt^{II}. In both cases, the rate of hydrosilylation will be faster if k_{ox}/k_{red} is larger. For strongly coordinating olefins, the oxidative addition of silane to Pt^0 will be disfavored,[9] and slower rates are expected. This conclusion is consistent with the observations by Kühn et al. that the rate constant for the hydrosilylation of 1-octene is larger than that for more strongly coordinating olefins such as norbornene.[9]

This mechanism also predicts that, for a mixture of two olefins, one that binds strongly to Pt^0 and one that binds weakly, the olefin that reacts first is the one that, in a noncompetitive experiment, is hydrosilylated more slowly. The more strongly coordinating olefin will react first because it binds more strongly to B and the intermediate C. This conclusion is consistent with our observation that, for a 1:9:5 mixture of AGE/1-octene/MD′M at 80 °C with **1-COD** as the precatalyst, AGE reaches full conversion to hydrosilylated products while 1-octene is largely left unreacted. The ability of AGE to bind to the metal center more strongly than 1-octene is the result of the epoxide oxygen atom, which enables AGE to chelate to the metal.

This mechanism also explains why DVTMS can serve as an inhibitor for the precatalyst **1-COD**. Kühn et al. have shown that DVTMS binds to Pt^0 more strongly than 1-octene. As a result, in a mixture of 1-octene and DVTMS, the latter will be the one that is bound to the intermediates in the catalytic cycle, and so it will be selectively hydrosilylated first despite the fact that, in separate experiments involving only a single olefin, DVTMS is hydrosilylated more slowly than 1-octene.

Note that DVTMS is not an effective inhibitor for Karstedt's catalyst.[9,10] It can be used as inhibitor for **1-COD** in the current system owing to the slow-release nature of **1-COD**; in other words, only a very small amount of generated Pt^0 needs to be inhibited, and DVTMS is able to do this.

CONCLUDING REMARKS

The platinum(II) ω-alkenyl complexes PtR_2, where R is $-CH_2SiMe_2CH{=}CH_2$ (**1**) or $-CH_2SiMe_2CH_2CH{=}CH_2$ (**2**), have been synthesized, along with the adducts **1-COD**, **1-NBD**, **1-DBCOT**, **2-COD**, and **2-DBCOT**, where COD = 1,5-cyclooctadiene, NBD = norbornadiene, and DBCOT = dibenzo[*a*,*e*]cyclooctatetraene. In **1** and **2**, the ω-alkenyl ligands are bidentate chelates, whereas in the diene adducts the ω-alkenyl ligands are unidentate. In solution, the C=C bonds in **1** and **2** reversibly decomplex at rates that are fast on the NMR time scale, and these two compounds are sensitive toward air, water, and heat. In contrast, the COD adducts, which are slow to lose COD, can be stored indefinitely in air. A TGA experiment shows that pure **1-COD** decomposes thermally at ∼100 °C.

1-COD, **1-NBD**, and **2-COD** show high activity for the hydrosilylation of a variety of olefin substrates when triggered by heat. Specifically, **1-COD** shows no reactivity for hours toward a number of substrates at 20 °C, but affords turnover numbers as high as 200000 at 50 °C after 4 h. The excellent product selectivity, absence of coloration, and the excellent anti-Markovnikov selectivity for typical olefin substrates—all of which are features seen for molecular platinum(0) carbene catalysts[10,11] suggest that in our system the formation of colloidal platinum is suppressed.

We find that the conversion of **1-COD** to molecular Pt^0 species follows a three-step "slow-release" mechanism: (1) slow dissociation of the bound COD from **1-COD** to generate an unstable Pt^{II} ω-alkenyl intermediate **1**. This step is rate determining. (2) Fast reaction of silane with the Pt^{II} ω-alkenyl intermediate **1** (e.g., by oxidative addition to form a Pt^{IV} silyl/hydride intermediate or by σ-complex-assisted metathesis, Scheme 9). (3) Fast elimination of L-H and L-SiR_3 to form the active catalyst (where L is the ω-alkenyl ligand). Step 1 is very slow at room temperature, but the rate increases

https://doi.org/10.1021/jacs.1c06846
J. Am. Chem. Soc. 2021, 143, 17492−17509

exponentially at higher temperatures. Steps 2 and 3 are highly efficient, and lead to near-quantitative generation of active Pt^0 catalyst, but the generation of this active catalyst is gradual owing to the slow-release nature of step 1. The slow dissociation of the bound COD also leads to latency. We also show that the latency of the catalysis can be tuned either by replacing the COD in **1-COD** with a different diene, or by addition of a consumable inhibitor to make the catalyst activation autoinductive, so that the rate accelerates quickly as the latency period ends.

The high turnover number and good selectivity can be also attributed to the slow-release nature of **1-COD** as a precatalyst. Compared to adding a source of Pt^0 all at once, adding **1-COD** to an olefin/silane mixture generates very small concentrations of Pt^0 in solution at the beginning of the catalysis, which disfavors the formation of unwanted colloidal Pt and reduces side reactions. Moreover, the slow-release nature of **1-COD** expands the scope of possible inhibitors and significantly reduces the amount of inhibitor needed to suppress premature curing.

For Karstedt's or Markó's catalyst, which are highly active even at room temperature, one substrate is typically added slowly to a mixture of the catalyst and the other substrate, so as to avoid a dangerous runaway exotherm. In contrast, because **1-COD** is almost inactive at room temperature but converts to an active catalyst at 50−80 °C, it can be added to a mixture of the two substrates, although caution is still warranted for neat reactions of reactive substrates on a large scale. As a result of these different experimental protocols, the turnover frequency in our system cannot be easily compared with those seen for Karstedt's or Markó's catalyst. But we know that **1-COD** converts to a "naked" Karstedt-like Pt^0 species; such species are known to be more reactive than Markó's catalyst.[10]

The precatalyst has a wide substrate scope and excellent anti-Markovnikov selectivity with minimal formation of side products such as isomerized olefins. The heat-triggered latent activity of makes **1-COD** potentially useful as a precatalyst to manufacture cross-linked silicone polymers for applications such as injection molding. The high reactivity, low catalyst loading, and good anti-Markovnikov selectivity seen for many olefin/silane substrate combinations also suggest that **1-COD** will be useful for solvent-free hydrosilylation reactions.

EXPERIMENTAL SECTION

All experiments were carried out in a vacuum or under argon using standard Schlenk techniques unless otherwise specified. All glassware was oven-dried before use. Solvents (pentane, diethyl ether) were distilled under nitrogen from sodium/benzophenone immediately before use. The silanes $HSiMe(OSiMe_3)_2$ (MD′M; Dow) and $HSiEt_3$ (Oakwood) were stored over 3 Å molecular sieves. The following starting materials were obtained from commercial sources (Sigma-Aldrich unless otherwise specified) and used as received: norbornadiene, diphenylacetylene (Aldrich), allyl glycidyl ether, 1-octene, vinyltriethoxysilane, allyl methacrylate, 2-methyl-3-butyn-2-ol, 3-vinyl-7-oxabicyclo[4.1.0]heptane (Oakwood). Benzene-d_6 was purchased from Cambridge Isotope Laboratories in 1 mL ampules. The 1D ^{1}H NMR data were recorded on a Varian Inova 400 spectrometer at 9.39 T, a Varian Inova 500 spectrometer at 11.74 T, a Varian Inova 600 spectrometer at 14.09 T, or a Bruker Avance III HD spectrometer equipped with a 5 mm BBFO CryoProbe at 11.74 T.

Only experiments directly related to hydrosilylation and the mechanism of activation of the precatalyst are reported here. For experimental details about the synthesis and characterization of the metal complexes, see the Supporting Information.

Hydrosilylation Reactions: General Protocol. The following is a typical procedure. To allyl glycidyl ether (0.59 mL, 5.0 mmol) was added bis[η^1-dimethyl(vinyl)silylmethyl](1,5-cyclooctadiene)-platinum(II) (10 μL of a 0.0012 M solution in benzene-d_6, 1.2×10^{-5} mmol, made by multiple stage dilution of the complex in benzene-d_6). After the mixture had been homogenized by shaking, MD′M (0.69 mL, 2.5 mmol) was added in one batch. The mixture was shaken again and then heated at 50 °C. Aliquots of the reaction mixture were removed at reaction times of 30 min, 4 h, and 24 h; the aliquots were immediately dissolved in benzene-d_6 to quench the reaction. The progress of the reaction was monitored by comparing the ^{1}H NMR integral of the residual Si−H resonance with those of the hydrosilylation products.

Hydrosilylation Reactions: Solvent-Free Conditions. Caution. Hydrosilylation reactions are highly exothermic. For neat (solventless) reactions on the scale described below, reactive substrates such as AGE can cause an exotherm of 15 °C; larger exotherms will occur at larger scales. The following is a typical procedure. To 1-octene (1.57 mL, 10.0 mmol) was added bis[η^1-dimethyl(vinyl)silylmethyl]-(1,5-cyclooctadiene)platinum(II), **1-COD** (40 μL of a 0.0012 M solution in benzene-d_6, 5×10^{-5} mmol). After the mixture was homogenized by shaking, MD′M (2.76 mL, 10 mmol) was added in one batch. The mixture was shaken again and then heated at 80 °C. Aliquots of the reaction mixture were removed at reaction times of 30 min, 4 h, and 24 h; the aliquots were immediately dissolved in benzene-d_6 to quench the reaction. The progress of the reaction was monitored by comparing the ^{1}H NMR integral of the residual Si−H resonance with those of the hydrosilylation products. After the reaction was complete, all volatile material was removed by sparging with dry air for 24 h. Because of the very low loading of platinum, the products remained colorless and no further purification was needed.

Kinetics of Hydrosilylation Reactions. To allyl glycidyl ether (1.18 mL, 10.0 mmol) was added a solution of **1-COD** (15 μL of a 0.008 M solution in benzene-d_6, 1.2×10^{-4} mmol). The mixture was homogenized by shaking, and to it was added triethylsilane (0.80 mL, 5.0 mmol). The mixture was again shaken and then placed in circulating oil bath preheated to 60 °C. At different reaction times, aliquots of the reaction mixture were taken out of the reaction mixture, and immediately dissolved in benzene-d_6 in an NMR tube; the NMR tube was immediately cooled to −78 °C to quench the reaction. The progress of the reaction was monitored by comparing the NMR integration of the residual Si−H resonance with the resonances of the hydrosilylation products.

The same procedure was used to measure the hydrosilylation reactions catalyzed by **1-NBD** stabilized by addition of 160 equiv of NBD (2.3×10^{-4} mmol).

Reaction between PtR_2 and MD′M. A solution of **1** (0.012 mmol) in pentane (0.25 mL) was evaporated to dryness under vacuum. The residue was cooled to −80 °C, and dry benzene-d_6 (0.65 mL) and diphenylacetylene (44.0 mg, 0.25 mmol) were added. The mixture was warmed to room temperature, the diphenylacetylene was dissolved with the aid of the stir bar, and MD′M (0.01 mL, ∼0.04 mmol) was added with vigorous stirring. The mixture was transferred to an NMR tube and a ^{1}H NMR spectrum was collected within 5 min of addition of silane. The reaction products were identified from ^{1}H NMR and GC−MS data. The reaction between **2** and MD′M was conducted in the same way.

Reaction between PtR_2COD and MD′M. **1-COD** and **2-COD** are stable toward air and water, so the reaction was conducted in air. Diphenylacetylene (44.0 mg, 0.25 mmol), **1-COD** (6.0 mg, 0.012 mmol), and benzene-d_6 (1 mL) were mixed in a vial. To this solution was added MD′M (0.01 mL, ∼0.04 mmol), and the solution was mixed and transferred to an NMR tube with a Pasteur pipet. The reaction was monitored by ^{1}H NMR spectroscopy over the course of a week. The reaction of **2-COD** with MD′M was conducted in the same way.

Reaction between PtR_2COD and MD′M. A stock solution of **1-COD** (15.0 mg, 0.030 mmol) in benzene-d_6 (1 mL) was prepared, and 100 μL of this solution was treated with a solution containing the desired amount of DBCOT (between 20 and 70 equiv) in benzene-d_6 (650 μL). The resulting solution was quickly mixed and transferred to an NMR tube, which was immediately inserted into the NMR spectrometer that had been equilibrated to desired temperature. The

https://doi.org/10.1021/jacs.1c06846
J. Am. Chem. Soc. 2021, 143, 17492−17509

sample was allowed to equilibrate in the probe temperature for 5 min, and then ^{1}H NMR spectra were acquired at desired time intervals; a recycle delay of 5 s was used to ensure quantitative analysis. The concentration of **1-COD** was monitored by the integration of the olefinic COD resonance.

■ ASSOCIATED CONTENT

Supporting Information

The Supporting Information is available free of charge at https://pubs.acs.org/doi/10.1021/jacs.1c06846.

Synthesis and characterizations of platinum compounds; ^{1}H, ^{13}C, ^{195}Pt, 2D NMR, and IR spectra of the platinum compounds; TGA data of **1**; experimental details about the solution behavior of **1** and **2**, including variable-temperature ^{1}H and ^{13}C{^{1}H} NMR spectra and resulting van't Hoff plots of the equilibrium between the C_2 and C_s isomers of **1** and **2**, variable-temperature ^{13}C{^{1}H} NMR line shape fits and resulting Eyring plots of the rate of exchange between the C_2 and C_s isomers of **1** and **2**; experimental details about the thermolysis of **1** and **2**, including kinetic plots, raw NMR/GC/mass spec data and product assignments of the products of thermolysis of **1**; NMR/GC/mass spec data and product assignments of the reaction products between of **1** and silane; kinetic plots, raw NMR/GC/mass spec data related to the thermolysis of **2** in C_6D_6 and reactivity of **2** with silane; NMR spectra and kinetic plots of the diene exchange reactions between COD adducts and DBCOT; characterization data of small molecule products and polymer products; crystallographic studies of **2**, **1-DBCOT**, **2-DBCOT**, and **4** (PDF)

Accession Codes

CCDC 2069185, 2069192−2069193, and 2093811 contain the supplementary crystallographic data for this paper. These data can be obtained free of charge via www.ccdc.cam.ac.uk/data_request/cif, or by emailing data_request@ccdc.cam.ac.uk, or by contacting The Cambridge Crystallographic Data Centre, 12 Union Road, Cambridge CB2 1EZ, UK; fax: +44 1223 336033.

■ AUTHOR INFORMATION

Corresponding Author

Gregory S. Girolami − *School of Chemical Sciences, University of Illinois at Urbana−Champaign, Urbana, Illinois 61801, United States;* orcid.org/0000-0002-7295-1775; Email: girolami@scs.illinois.edu

Author

Sumeng Liu − *School of Chemical Sciences, University of Illinois at Urbana−Champaign, Urbana, Illinois 61801, United States;* Present Address: Department of Chemistry, University of California at Riverside, Riverside, CA 92521; orcid.org/0000-0002-2133-2122

Complete contact information is available at: https://pubs.acs.org/10.1021/jacs.1c06846

Author Contributions

All authors have given approval to the final version of the manuscript.

Notes

The authors declare the following competing financial interest(s): One patent application related to this work has been filed: Metal Complexes for Depositing Films and Method of Making and Using the Same, U.S. Patent 20200346197A1 (Published Nov. 5, 2020).

■ ACKNOWLEDGMENTS

We thank the Dow Chemical Co. and the National Science Foundation under Grant No. CHE 19-54745 (to G.S.G.) for support of this research and Dow scientists Dr. Matthew Jeletic and Dr. Dimitris Katsoulis for helpful discussions. We thank Dr. Danielle Gray and Dr. Toby Woods of the G. L. Clark X-ray Laboratory at the University of Illinois at Urbana−Champaign for help in collecting the X-ray diffraction data. We thank Professor Damien S. Guironnet and Dr. Dylan Walsh for conducting the GPC analysis.

■ REFERENCES

(1) Troegel, D.; Stohrer, J. Recent Advances and Actual Challenges in Late Transition Metal Catalyzed Hydrosilylation of Olefins from an Industrial Point of View. *Coord. Chem. Rev.* **2011**, *255*, 1440−1459.

(2) Jagadeesh, M. N.; Thiel, W.; Köhler, J.; Fehn, A. Hydrosilylation with Bis(alkynyl)(1,5-cyclooctadiene)platinum Catalysts: A Density Functional Study of the Initial Activation. *Organometallics* **2002**, *21*, 2076−2087.

(3) Hofmann, R. J.; Vlatković, M.; Wiesbrock, F. Fifty Years of Hydrosilylation in Polymer Science: A Review of Current Trends of Low-Cost Transition-Metal and Metal-Free Catalysts, Non-Thermally Triggered Hydrosilylation Reactions, and Industrial Applications. *Polymers* **2017**, *9*, 534.

(4) Nakajima, Y.; Shimada, S. Hydrosilylation Reaction of Olefins: Recent Advances and Perspectives. *RSC Adv.* **2015**, *5*, 20603−20616.

(5) Marciniec, B.; Maciejewski, H.; Pietraszuk, C.; Pawluc, P.*Hydrosilylation*; Springer Netherlands: Dordrecht, The Netherlands, 2009.

(6) Obligacion, J. V.; Chirik, P. J. Earth-abundant transition metal catalysts for alkene hydrosilylation and hydroboration. *Nature Reviews Chemistry* **2018**, *2*, 15−34.

(7) Lewis, L. N.; Stein, J.; Gao, Y.; Colborn, R. E.; Hutchins, G. Platinum Catalysts Used in the Silicones Industry. Their Synthesis and Activity in Hydrosilylation. *Platinum Metals Rev.* **1997**, *41*, 66−75.

(8) Hitchcock, P. B.; Lappert, M. F.; Warhurst, N. J. W. Synthesis and Structure of a rac-Tris(divinyldisiloxane) diplatinum(0) Complex and its Reaction with Maleic Anhydride. *Angew. Chem., Int. Ed. Engl.* **1991**, *30*, 438−440.

(9) Meister, T. K.; Riener, K.; Gigler, P.; Stohrer, J.; Herrmann, W. A.; Kühn, F. E. Platinum Catalysis Revisited—Unraveling Principles of Catalytic Olefin Hydrosilylation. *ACS Catal.* **2016**, *6*, 1274−1284.

(10) Markó, I. E.; Stérin, S.; Buisine, O.; Mignani, G.; Branlard, P.; Tinant, B.; Declercq, J.-P. Selective and Efficient Platinum(0)-Carbene Complexes As Hydrosilylation Catalysts. *Science* **2002**, *298*, 204.

(11) Dierick, S.; Vercruysse, E.; Berthon-Gelloz, G.; Markó, I. E. User-Friendly Platinum Catalysts for the Highly Stereoselective Hydrosilylation of Alkynes and Alkenes. *Chem. - Eur. J.* **2015**, *21*, 17073−17078.

(12) Sigeev, A. S.; Peregudov, A. S.; Cheprakov, A. V.; Beletskaya, I. P. The Palladium Slow-Release Pre-Catalysts and Nanoparticles in the "Phosphine-Free" Mizoroki−Heck and Suzuki−Miyaura Reactions. *Adv. Synth. Catal.* **2015**, *357*, 417−429.

(13) Roy, A. K.; Taylor, R. B. The First Alkene−Platinum−Silyl Complexes: Lifting the Hydrosilation Mechanism Shroud with Long-Lived Precatalytic Intermediates and True Pt Catalysts. *J. Am. Chem. Soc.* **2002**, *124*, 9510−9524.

(14) Stein, J.; Lewis, L. N.; Gao, Y.; Scott, R. A. In Situ Determination of the Active Catalyst in Hydrosilylation Reactions Using Highly Reactive Pt(0) Catalyst Precursors. *J. Am. Chem. Soc.* **1999**, *121*, 3693−3703.

(15) Plasson, R.; Brandenburg, A.; Jullien, L.; Bersini, H. Autocatalyses. *J. Phys. Chem. A* **2011**, *115*, 8073−8085.

(16) Kelly, R. D.; Young, G. B. Synthesis and Spectroscopic Characteristics of Bis(ethenyldimethylsilylmethyl)platinum(II) Complexes Containing Tertiary Phosphine Ligands. *Polyhedron* **1989**, *8*, 433−445.
(17) Kelly, R. D.; Young, G. B. Synthesis and Spectroscopic Characteristics of Bis(ethenyldimethylsilylmethyl)platinium(II) Complexes Containing Nitrogen Donor Ligands. *J. Organomet. Chem.* **1989**, *361*, 123−138.
(18) Liu, S.; Zhang, Z.; Gray, D.; Zhu, L.; Abelson, J. R.; Girolami, G. S. Platinum ω-alkenyl Compounds as Chemical Vapor Deposition Precursors. Synthesis and Characterization of $Pt[CH_2CMe_2CH_2CH{=}CH_2]_2$ and the Impact of Ligand Design on the Deposition Process. *Chem. Mater.* **2020**, *32*, 9316−9334.
(19) Wyrwa, R.; Poppitz, W.; Görls, H. Massenspektrometrische und Röntgenstrukturanalytische Untersuchungen an Komplexen des Typs $(COD)PtX_2$ (X = Cl, Br, I, CH_3, CH_2CMe_3, CH_2SiMe_3). *Z. Anorg. Allg. Chem.* **1997**, *623*, 649−653.
(20) Wierschke, S. G.; Chandrasekhar, J.; Jorgensen, W. L. Magnitude and Origin of the β-Silicon Effect on Carbenium Ions. *J. Am. Chem. Soc.* **1985**, *107*, 1496−1500.
(21) Brinkman, E. A.; Berger, S.; Brauman, J. I. α-Silyl-Substituent Stabilization of Carbanions and Silyl Anions. *J. Am. Chem. Soc.* **1994**, *116*, 8304−8310.
(22) Wetzel, D. M.; Brauman, J. I. Quantitative Measure of α-Silyl Carbanion Stabilization. The Electron Affinity of (Trimethylsilyl)-methyl Radical. *J. Am. Chem. Soc.* **1988**, *110*, 8333−8336.
(23) Larson, G. L.*Advances in Silicon Chemistry*; JAI Press: Greenwich, CT, 1996.
(24) Ankianiec, B. C.; Christou, V.; Hardy, D. T.; Thomson, S. K.; Young, G. B. Mechanisms of Thermolytic Rearrangement of *cis*-Bis(silylmethyl)platinum(II) Complexes: β-Carbon Transfer Predominates over Hydrogen Transfer. *J. Am. Chem. Soc.* **1994**, *116*, 9963−9978.
(25) Stoebenau, E. J.; Jordan, R. F. Nonchelated Alkene and Alkyne Complexes of d^0 Zirconocene Pentafluorophenyl Cations. *J. Am. Chem. Soc.* **2006**, *128*, 8638−8650.
(26) Carpentier, J.-F.; Wu, Z.; Lee, C. W.; Strömberg, S.; Christopher, J. N.; Jordan, R. F. d^0 Metal Olefin Complexes. Synthesis, Structures, and Dynamic Properties of $(C_5R_5)_2Zr(OCMe_2CH_2CH_2CH{=}CH_2)^+$ Complexes: Models for the Elusive $(C_5R_5)_2Zr(R)(Olefin)^+$ Intermediates in Metallocene-Based Olefin Polymerization Catalysis. *J. Am. Chem. Soc.* **2000**, *122*, 7750−7767.
(27) Carpentier, J.-F.; Maryin, V. P.; Luci, J.; Jordan, R. F. Solution Structures and Dynamic Properties of Chelated d^0 Metal Olefin Complexes $\{\eta^5{:}\,\eta^1\text{-}C_5R_4SiMe_2NtBu\}Ti(OCMe_2CH_2CH_2CH{=}CH_2)^+$ (R = H, Me): Models for the $\{\eta^5{:}\,\eta^1\text{-}C_5R_4SiMe_2NtBu\}Ti(R')(olefin)^+$ Intermediates in "Constrained Geometry" Catalysts. *J. Am. Chem. Soc.* **2001**, *123*, 898−909.
(28) Casey, C. P.; Carpenetti, D. W. Measurement of Barriers for Alkene Dissociation and for Inversion at Zirconium in a d^0 Zirconium−Alkyl−Alkene Complex. *Organometallics* **2000**, *19*, 3970−3977.
(29) Casey, C. P.; Carpenetti, D. W.; Sakurai, H. Models for Intermediates in Metallocene-Catalyzed Alkene Polymerization: Alkene Dissociation from $Cp_2Zr[\eta^1,\eta^2\text{-}CH_2Si(CH_3)_2CH_2CH{=}CH_2]\text{-}[B(C_6F_5)_4]$. *Organometallics* **2001**, *20*, 4262−4265.
(30) Neugebauer, M.; Schmitz, S.; Krause, M.; Nikos, L. D.; Klein, A. Reactions of the Organoplatinum Complex [Pt(cod)(neoSi)Cl] (neoSi = Trimethylsilylmethyl) with the non-Coordinating Anions SbF_6^- and BPh_4^-. *Open Chem.* **2018**, *16*, 1214.
(31) Thomson, S. K.; Young, G. B. Thermolytic Rearrangement of *cis*-Bis(phosphine)bis((trimethylsilyl)methyl)platinum(II) Complexes via b-Alkyl Transfer. *Organometallics* **1989**, *8*, 2068−2070.
(32) Chisholm, M. H.; Clark, H. C.; Manzer, L. E.; Stothers, J. B.; Ward, J. E. H. Carbon-13 Nuclear Magnetic Resonance Studies of Organometallic Compounds. VII. 1,5-Cyclooctadieneplatinum(II) Derivatives. *J. Am. Chem. Soc.* **1975**, *97*, 721−727.
(33) Jeffery, J.; Lappert, M. F.; Luong-Thi, N. T.; Webb, M.; Atwood, J. L.; Hunter, W. E. Metallocene Derivatives of Early Transition Metals. Part 4. Chemistry of the Complexes $[M(\eta\text{-}C_5H_5)_2RR'][M = Ti, Zr, or Hf; R = CH_2M'Me_3(M' = C, Si, Ge, or Sn) or CH(SiMe_3)_2; R' = Cl or alkyl]$ and the X-ray Structures of $[Zr(\eta\text{-}C_5H_5)_2(CH_2M'Me_3)_2](M' = C or Si)$. *J. Chem. Soc., Dalton Trans.* **1981**, 1593−1605.
(34) Faglioni, F.; Blanco, M.; Goddard, W. A.; Saunders, D. Heterogeneous Inhibition of Homogeneous Reactions: Karstedt Catalyzed Hydrosilylation. *J. Phys. Chem. B* **2002**, *106*, 1714−1721.
(35) Su, W.-F., Step Polymerization. In *Principles of Polymer Design and Synthesis*; Su, W.-F., Ed.; Springer: Berlin, 2013; pp 111−136.
(36) The amount of internal olefin formed depends on the olefin and on the choice of silane; they play no role further in the catalysis. These internal olefin products are highly volatile and can be easily removed from product mixture.
(37) Whitesides, G. M.; Hackett, M.; Brainard, R. L.; Lavalleye, J. P. P. M.; Sowinski, A. F.; Izumi, A. N.; Moore, S. S.; Brown, D. W.; Staudt, E. M. Suppression of Unwanted Heterogeneous Platinum(0)-Catalyzed Reactions by Poisoning with Mercury(0) in Systems Involving Competing Homogeneous Reactions of Soluble Organoplatinum Compounds: Thermal Decomposition of Bis(triethylphosphine)-3,3,4,4-tetramethylplatinacyclopentane. *Organometallics* **1985**, *4*, 1819−1830.
(38) Tagge, C. D.; Simpson, R. D.; Bergman, R. G.; Hostetler, M. J.; Girolami, G. S.; Nuzzo, R. G. Synthesis of a Novel Volatile Platinum Complex for Use in CVD and a Study of the Mechanism of Its Thermal Decomposition in Solution. *J. Am. Chem. Soc.* **1996**, *118*, 2634−2643.
(39) Lewis, L. N.; Colborn, R. E.; Grade, H.; Bryant, G. L.; Sumpter, C. A.; Scott, R. A. Mechanism of Formation of Platinum(0) Complexes Containing Silicon-Vinyl Ligands. *Organometallics* **1995**, *14*, 2202−2213.
(40) Chalk, A. J.; Harrod, J. F. Homogeneous Catalysis. II. The Mechanism of the Hydrosilation of Olefins Catalyzed by Group VIII Metal Complexes. *J. Am. Chem. Soc.* **1965**, *87*, 16−21.
(41) Fitch, J. W.; Brown, M.; Hall, N. H.; Mebe, P. P.; Owens, K. A.; Roesch, M. R. Hydrolysis of Allylsilanes Coordinated to Platinum(II). *J. Organomet. Chem.* **1983**, *244*, 201−207.
(42) Perutz, R. N.; Sabo-Etienne, S. The σ-CAM Mechanism: σ Complexes as the Basis of σ-Bond Metathesis at Late-Transition-Metal Centers. *Angew. Chem., Int. Ed.* **2007**, *46*, 2578−2592.
(43) Tsutsumi, H.; Sunada, Y.; Nagashima, H. Novel Disilaplatina-cyclopentenes Bearing Dialkylsulfide Ligands: Preparation, Characterization, and Mechanistic Consideration of Hydrosilane Reduction of Carboxamides by Bifunctional Organohydrosilanes. *Organometallics* **2011**, *30*, 68−76.
(44) Contrary to **1-COD**, which shows <5% conversion after 4 h, addition of MD′M to **2-COD** leads to the formation of 5% $Pt(DPA)_2$ within 30 min without the formation of a corresponding amount of COD. Notably, the conversion increases only slightly to 5.2% after 4 h. The initial rapid conversion to Pt^0 is due to the presence of small amount of free **2** as a minor (4%) component of isolated samples of **2-COD** (see SI). This is likely because **2** is more stable than **1**, and a small amount of **COD** is lost during the isolation of **2-COD**.
(45) Rivero-Crespo, M.; Oliver-Meseguer, J.; Kapłońska, K.; Kuśtrowski, P.; Pardo, E.; Cerón-Carrasco, J. P.; Leyva-Pérez, A. Cyclic Metal(oid) Clusters Control Platinum-Catalysed Hydrosilylation Reactions: from Soluble to Zeolite and MOF Catalysts. *Chem. Sci.* **2020**, *11*, 8113−8124.

https://doi.org/10.1021/jacs.1c06846
J. Am. Chem. Soc. 2021, 143, 17492−17509